LYSENIN CHANNELS AS SINGLE MOLECULE NANO-SENSORS AND NANO-SWITCHES FOR CONTROLLED MEMBRANE PERMEABILITY

by

Nisha Shrestha

A dissertation

submitted in partial fulfillment

of the requirements for the degree of

Doctor of Philosophy in Biomolecular Sciences

Boise State University

August 2017

BOISE STATE UNIVERSITY GRADUATE COLLEGE

DEFENSE COMMITTEE AND FINAL READING APPROVALS

of the dissertation submitted by

Nisha Shrestha

Dissertation Title: Lysenin Channels as Single Molecule Nano-Sensors and Nano-Switches for Controlled Membrane Permeability

Date of Final Oral Examination: 27th June 2017

The following individuals read and discussed the dissertation submitted by student Nisha Shrestha, and they evaluated her presentation and response to questions during the final oral examination. They found that the student passed the final oral examination.

Daniel Fologea, Ph.D.	Co-Chair, Supervisory Committee
Juliette Tinker, Ph.D.	Co-Chair, Supervisory Committee
Denise Wingett, Ph.D.	Member, Supervisory Committee
Xinzhu Pu, Ph.D.	Member, Supervisory Committee
James R. Groome, Ph.D.	External Examiner

The final reading approval of the dissertation was granted by Daniel Fologea, Ph.D. and Juliette Tinker, Ph.D., Co-Chairs of the Supervisory Committee. The dissertation was approved by the Graduate College.

DEDICATION

To my beloved parents and my lovely husband.

ACKNOWLEDGEMENTS

The completion of this dissertation would not have been possible without support from many individuals. Foremost, I would like to express immense gratitude to my amazing advisor Dr. Daniel Fologea, who not only encouraged and supported me, but also provided me with all the freedom and flexibility to carry out my research projects. His enthusiasm, intelligence, passion, contagious energy, and cheerful personality have always been my motivational force and have made all of these years a pleasant journey. My ambition of getting a doctoral degree would not have been possible if he hadn't welcomed me in his lab, believed in me and my ability to succeed. I am indebted to him forever for all the tremendous support he bestowed on me during my Ph.D. endeavor. I would also like to extend my heartfelt gratitude to my other advisor, Dr. Juliette Tinker, for her invaluable advice, dedication, and friendly nature. Her support and motivation have always provided me with confidence to move forward with my graduate degree. I would also like to thank Dr. Denise Wingett for her expert advice, support, encouragement, and her warm welcoming personality. I would like to deeply acknowledge Dr. Xinzhu Pu for his meticulous training with mass spectroscopy techniques and all his guidance and support during my Ph.D. training.

My graduate journey would have been a turbulent voyage without the financial support from the Biomolecular Sciences Graduate Program and the Biomolecular Research Center (BRC) at Boise State University. My sincere thanks to the BRC for two years of fellowships and all of the generous grants, training, and support, without which

the completion of my research would not have been possible. I would like to thank Raquel Brown for training me in confocal microscopy, and for all of her warmness and supportive nature. I am also grateful to Dr. Julie Oxford for supporting me in my graduate endeavor. My deepest and sincere thanks to Dr. Rebecca Hermann for her help with my Jurkat cells experiments and for training me in flow cytometry. My time at Boise State University would not have been enjoyable without my extremely amusing and incredibly smart colleagues Sheenah Bryant, Christopher Thomas, Devon Richtsmeier, Madhu Kongara, Eric Krueger, Philip Belzeski, Samuel Kosydar, Lizzie Leung, Daniel Prather, and Josh Eixenberger. I would especially like to thank my two incredibly talented friends Chris and Devon for helping me with my research projects. I am also grateful to Beth Gee for making my life easier with all of her help behind the scenes with paperwork and travel grants as well as listening to my frustrations from time to time. I would also like to express my heartfelt gratitude to the Department of Physics for all the help and support during these four years.

Finally, I want to enormously thank my lovely parents and my gleeful husband for their continuous love, support, blessing, and motivation. Without them, I would not have been here pursuing my dream to become a scientist.

ABSTRACT

Pore-forming toxins secreted by various evolutionarily distant organisms are important components of their innate defense mechanisms. These toxins may kill the target cells by inserting un-regulated channels into the plasma membrane. Tampering with the otherwise well-controlled membrane permeability alters cell homeostasis by contributing to un-controlled dissipation of both chemical and electrical gradients, which is often an essential component of virulence mechanisms leading to cell death. However, the same ability to create nanoscopic conducting pathways, i.e. nanopores, has been exploited for creating powerful tools in nano-biotechnology. Single nano-channels reconstituted in artificial planar lipid membranes are extremely versatile sensors that are capable of detection, identification, and characterization of single molecules. In addition, the changes in permeability induced by pore-forming toxins reconstituted in artificial and natural lipid membrane systems are exploited for numerous biomedical, scientific, and bio-technological applications. Many of these applications, underlying principles, and limitations are briefly described in the introduction section of this dissertation.

To overcome many of the restrictions presented by currently used pore-forming toxins, we propose to use lysenin channels for both stochastic sensing and for the achievement of controlled membrane permeability. Lysenin is a pore-forming toxin extracted from the earthworm *E. foetida* that inserts large nanopores in natural and artificial lipid membranes containing sphingomyelin. Chapter 2 of the presented work is focused on exploring the use of single lysenin nanopores for stochastic sensing of human

angiotensin II, a short hormone peptide,which is highly relevant for the pathophysiology of cardiovascular diseases. Besides a traditional analysis of the interactions between lysenin channels and peptides, we succeeded to employ high sensitivity liquid chromatography – mass spectroscopy analyses to demonstrate the passage of un-altered peptide molecules through open lysenin channels.

In Chapter 3 we exploit the unique regulatory mechanisms presented by lysenin channels to achieve controlled permeability over artificial and natural lipid membranes. We demonstrate that ATP molecules may reversibly regulate the macroscopic ionic conductance of lysenin channels inserted into planar lipid membranes. Lysenin reconstitution into spherical membranes (liposomes) enables a two-way control over membrane permeability by using multivalent metal cations capable of inducing reversible ligand-induced gating of the channels. Live cell analyses demonstrate that lysenin channels allow transport of non-permeant molecules in Jurkat leukemia and ATDC5 chondrogenic cells. In addition, extended control over membrane permeability is achieved by using chitosan molecules as irreversible blockers of the macroscopic conductance. Survival rate estimations indicate that the permeabilized cells maintain a satisfactory viability rate for further use. Therefore lysenin may be used for the controlled transport of ions and molecules in living systems.

TABLE OF CONTENTS

LIST OF FIGURES

CHAPTER ONE

CHAPTER TWO

CHAPTER THREE

LIST OF ABBREVIATIONS

Ang II	angiotensin II
Aso	asolectine
ATP	adenosine triphosphate
α-HL	α-Hemolysin
BLM	bilayer lipid membrane
Chol	cholesterol
DMEM/F12	Dulbecco's modified Eagle's medium: nutrient mixture F-12
E. coli	*Escherichia coli*
EtHD	ethidium homodimer-1
ESI	electrospray ionization
FBS	fetal bovine serum
GBCD	glass bottom culture dishes
HBSS	Hank's balanced salt solution
$<I_B>$	average current change
LC-MS	liquid chromatography – mass spectroscopy
MscL	mechanosensitive channel L
MspA	mycobacterium smegmatis porin A
OmpF	outer membrane protein F
Q-TOF	quadruple-time-of-flight
PEG	poly-ethylene glycol
PFPs	pore-forming proteins

PFTs	pore-forming toxins
PI	propidium iodide
PTFE	polytetrafluoroethylene
SM	sphingomyelin
t_D	dwell time
TEM	transmission electron microscopy

CHAPTER ONE: BIOLOGICAL NANOPORES AND THEIR APPLICATIONS FOR SENSING AND CONTROLLED TRANSPORT

Introduction and Background

Protein channels

Protein channels are ubiquitous transmembrane elements capable of transporting ions and molecules across artificial and natural lipid membranes [1-6]. Their ability to overcome the barrier function of the membrane stems from the establishment of tiny conducting pathways between the aqueous solutions bathing the two sides of the membrane. Protein channels are essential for cellular activities, including creating and maintaining electrochemical gradients, producing energy, and enabling communication [1-6]. To ensure such complex functionalities, numerous protein channels are regulated by physical and chemical stimuli that modulate their transport properties. Typical examples are ion channels, which are necessary for the correct functionality of all cells. Ion channels are passive and selective transporters controlled by external stimuli that act upon them and modulate the electrical conductance and transport capabilities [7-9]. A special class of transmembrane transporters consists of pore-forming toxins (PFTs), which are among the most studied and well-understood class of membrane–binding proteins [10-14]. Mostly of bacterial origin, PFTs significantly contribute to bacterial virulence by targeting and inserting into host cell membranes. Consequently, PFTs comprise about 25% of all known protein toxins of bacterial origin [11]. However, they may be secreted by multiple organisms such as amoeba [12], cnidarian [13], earthworm

[14], sea anemones [15], plants [16, 17] and even humans [18]. A salient feature of all PFTs is that their interaction with components in lipid membranes leads to damage manifested as an increase in permeability. The mechanism by which the membrane barrier function is affected relies on their reconstitution into nano-sized transmembrane pathways, or nanopores, which endow the target membrane with novel permeation pathways and establish electrical connections. This feature has not escaped the attention of scientists, who have explored and developed nanopore-based technologies to vertically advance science, technology and medicine. Nanopores provide novel approaches for biosensing, single molecule detection and characterization, sequencing, diagnosis, drug delivery, and controlling membrane permeability [19-27]. Although these advances rely on the ability of PFTs to introduce transmembrane conducting pathways, the biological materials and associated methodologies are specifically tailored to each application, as outlined in the following subsections.

The resistive pulse technique at the nano-scale

Current nano-sensing approaches based on the resistive pulse technique rely on the deceptively simple Coulter principle developed decades ago [28]. A small hole perforated in an electrically insulating material which separates two electrolyte-filled reservoirs constitute the only electrical pathway through which an ionic current may be established under application of an external voltage. When a particle moves through the conducting pathway, it temporarily reduces the ionic flow and increases the electrical resistance (resistive pulse), which is translated into a measurable decrease in ionic current for the duration of the passage. The magnitude of the change in conductance is equated to the size of the passing particle, making particle counting and size distribution

measurements achievable. While biomedical and industrial applications benefit from practical implementations of the Coulter principle, scientists began to investigate its potential extension at the molecular level. The success of such an approach was dependent upon the establishment of conducting pathways sized similarly to the molecules under investigation. Since synthetic nanopores were not available [29], explorations focused on using biological nanopores inserted into artificial lipid membranes. As depicted in Figure 1, a typical nano-sensing device includes single channels inserted into a bilayer lipid membrane (BLM) created in a hole made in a hydrophobic film separating two electrolyte-filled reservoirs. The BLM serves as both support for the inserted channels and the insulating partition between the conducting solutions bathing it, such that the inserted nanopores are the only conducting pathways between the two sides. The electrical connections established with Ag/AgCl electrodes embedded in each of the reservoirs are used to apply the external driving voltage and to measure the ionic currents through the channels by using sensitive amplifiers.

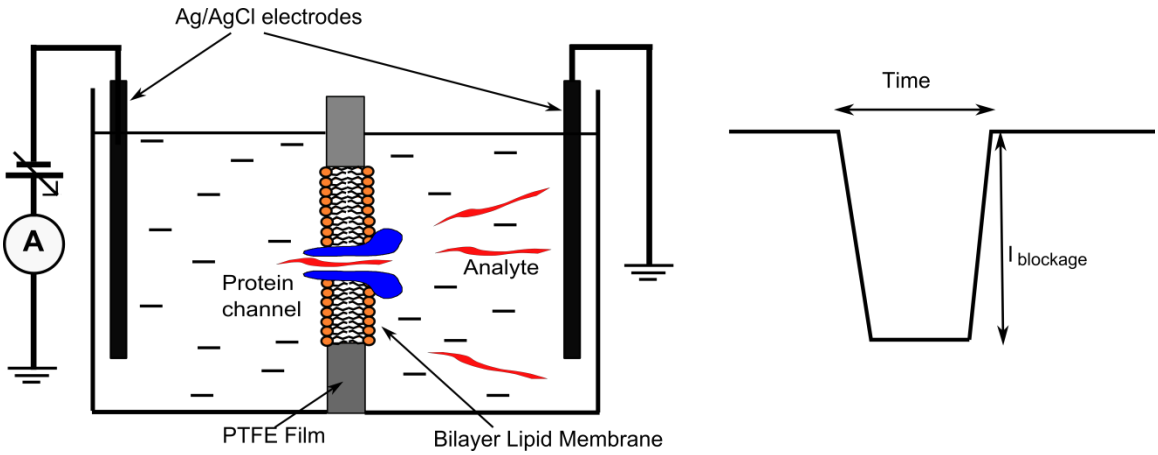

Figure 1. The planar bilayer membrane set up. A lipid bilayer is formed in a tiny hole in a polytetrafluorethylene (PTFE) film that separates the two electrolyte solutions. The electrical connection is achieved by Ag/AgCl electrodes. The insertion of single channels into a lipid bilayer membrane establishes the electrical connection. The analytes can be identified, detected, or characterized on the basis of current blockade and duration under the external electric field.

The principle of measuring at the nano-scale utilizes the Coulter principle and is based on the analysis of the transient changes in ionic currents produced by the partial occlusion of the conducting pathway during the passage of molecules. The original Coulter approach employs a method of pushing the particles through the orifice by pumping, which is not a valid option for the fragile membrane created between the two reservoirs. Although diffusion alone may force neutral molecules to thread the nanopore, the large entropic penalty presented by the small channel opening may significantly reduce the rate of molecules translocated between the two sides. Partial compensation by increasing the analyte concentration is not always feasible owing to the limited availability or potential undesired interactions with the lipid membrane. Nonetheless, many biomolecules are electrically charged, which present the opportunity to electrophoretically drive the molecules through the nanopore. This development allowed Kasianowicz *et al.* to demonstrate, for the first time, the translocation of single-stranded DNA (ssDNA) molecules through a single alpha-hemolysin nanopore (α-HL, a water

soluble toxin from *Staphylococcus aureus*) and to propose the use of nanopore-based sensing for next generation sequencing [30-38]. Since this revolutionary discovery, several other biological nanopores have been proposed for derived applications, such as macromolecule detection and characterization, interaction studies, identification of pathogens, diagnosis, controlled drug delivery, and nucleic acids and protein sequencing [22, 27, 39].

Translocation studies using biological nanopores

In 1996, the study of α-HL for the passage of single-stranded DNA (ssDNA) or RNA by Kasianowicz *et al.*, using the resistive pulse technique, led to a revolution in the field of nanopore technology [30]. Since then, nanopores have been widely explored for single molecule identification and characterization, sequencing, conformational analysis, orientation determination, and to study the interactions of molecules. α-HL, the most commonly used nanopore, is a mushroom-shaped, long, heptameric, β-barrel transmembrane protein of 10 nm height and has a diameter in the range of 1.4–2.6 nm (Figure 2) [40]. The α-HL nanopore is able to distinguish between purine and pyrimidine homo-polymers based on their characteristic features that include dwell time and current blockage, leading scientists to envision its use for sequencing purposes [31, 41]. The long β-barrel, which can accommodate ~10-15 nucleotides, and the high speed of the analyte through the pore during translocation preclude individual nucleotide recognition. However, addition of chemical tags to specific nucleotides improves the spatial resolution and enables base-specific identification [42].

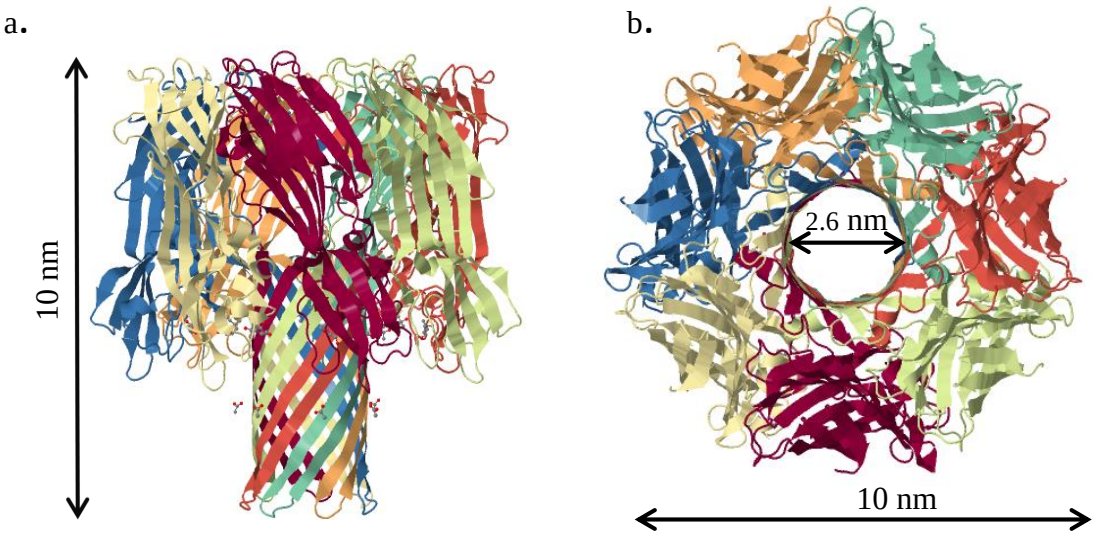

Figure 2. Structure of α-HL. a) α-HL is a mushroom shaped β-barrel protein of height 10 nm. b) The top view of the structure indicates the seven subunits (shown in different color) with the pore diameter of ~ 2.6 nm. The protein is also characterized by the presence of a vestibule and the narrow constriction of size ~ 1.5 nm (which is not shown in the figure). Adapted from Song et al. (1996), PDB 3ANZ [40])

An improvement in the ability to identify the four DNA nucleotides is achieved by using biotinylated ssDNA conjugated with streptavidin and nucleotide recognition sites present in the lumen of the α-HL nanopore [43]. However, this approach precluded full translocation of the conjugated DNA molecule, which was immobilized by α-HL nanopores. The magnitude of the residual currents achieved after immobilization is sequence-dependent [43]. Further improvements of this approach aimed at enhancing the energy barrier for ion movement and demonstrated an improved ability for base discrimination [44]. Another approach utilizes the synthesis method where a DNA-polymerase complex is attached to the nanopore and, during DNA synthesis, the distinct tags from the complementary-nucleotide enter the pore and provides unique electronic signatures for accurate base discrimination [45, 46]. A different strategy employs conjugating an *E.coli* exonuclease to a nanopore [47]. The nuclease cleaves the

nucleotides, which are further detected during translocation through the nanopore, narrowed by introducing an amino-β-cyclodextrin ring as a molecular adapter. All these advancements led to the launching of a first device intended for nanopore sequencing (MinIon) by Oxford Nanopore Technologies in 2014 [19, 48].

Although α-HL has received the most attention in the field of nanotechnology for sequencing purposes, other nanopores have emerged as promising tools for nanopore based sequencing. For example, *Mycobacterium smegmatis* porin A (MspA) is an octameric bacterial porin that has a constriction of 1.2 nm and a length of 9.6 nm (Figure 3) [49]. The presence of the narrow constriction equipped MspA with improved spatial resolution compared to α-HL. An engineered MspA was first demonstrated in 2008 for the detection of ssDNA molecules [50]. The immobilization of ssDNA inside the MspA nanopore, either by using complementary strands or biotin-neutravidin complex, allows discrimination between the four nucleotides [51, 52]. Similar to the study using α-HL, the combination of engineered MspA with phi29 DNA polymerase provided the discrimination of nucleotides with a good correlation between the current pattern and known DNA sequence and implicated MspA as one of the strong aspirants in the race of nanopore-based sequencing [53].

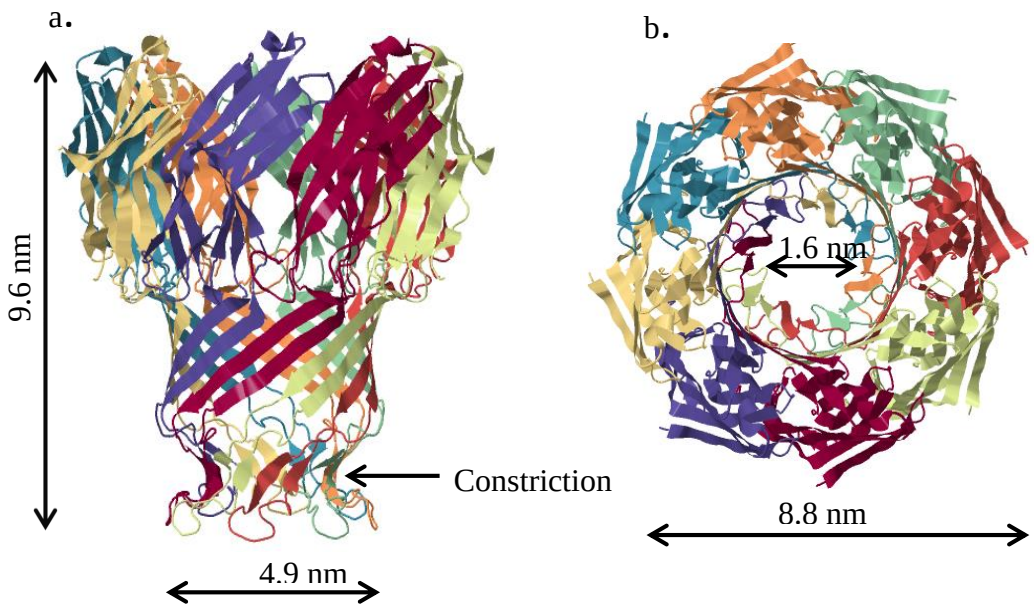

Figure 3. Structure of the MspA pore. a) MspA is an octameric β-barrel of height ~9.6 nm and characterized by the presence of a small constriction. b) The top view shows the eight subunits and constriction of diameter ~1.6 nm. (Adapted from Faller et al. (2004), PDB 1UUN [49])

Even though nanopores have been mostly exploited for the development of rapid, accurate, and inexpensive sequencing tools, scientists have also found applications for other purposes. The α-HL nanopore can be used for the characterization of neutral molecules such as poly-ethylene glycol (PEG) [54]. The translocation of PEG of different molecular masses produces distinct current drops and residence times. Further analysis suggests that the characteristic features generated from the passage of different PEG sizes depend on the mobile cation concentration inside the pore and the attractive interaction between the pore and polymer [55]. In addition, both α-HL and MspA have demonstrated the potential to identify epigenetic markers including 5-methylcytosine and 5-hydroxymethylcytosine in DNA strands [26, 56]. α-HL has also been investigated for the identification and detection of chemically-modified nucleotides, mismatches, base pairing of oxidized bases in duplex DNA, or to characterize the inter-strand cross-link in duplex

DNA [57-60]. Besides polynucleotides, protein nanopores were also explored for the translocation and characterization of peptides and proteins, which may provide novel tools for peptide sequencing and structure determination [61-63]. The rate constant obtained from the transport of cationic peptides through α-HL depends on the applied transmembrane voltage and peptide length, thereby adding other parameters for the characterization of polypeptides using nanopores [61]. Also, the charges inside of the pore can significantly affect the association and dissociation constant during the translocation of cationic polypeptides by altering the energy barrier [64]. Translocation of partially folded and unfolded maltose-binding proteins through α-HL in the presence of denaturing agents suggested that completely unfolded proteins produce short blockades while partially folded proteins give rise to long blockades [65]. Folded and unfolded peptides with β-hairpins demonstrated similar effects supporting the use of α-HL for studying the structure of proteins [66]. Proteins were also translocated via α-HL facilitated by an unfoldase enzyme, where the enzyme unfolds and translocate the protein in an ATP-dependent manner [67].

Aerolysin, a pore-forming toxin secreted by *Aeromonas hydrophila*, was employed for the characterization of polymers including polynucleotides and polypeptides. It forms a vestibule-less mushroom-shaped heptameric β-barrel pore of a diameter approximately 1.0 – 1.7 nm (Figure 4) [68-70]. Aerolysin was first employed in 2006 as an analysis tool for translocation of α-helical peptides [62]. Since this time, aerolysin has found applications in the study and characterization of oligo/polynucleotides [71, 72], chimera proteins [73], proteins [74-76], and oligosaccharides [77, 78].

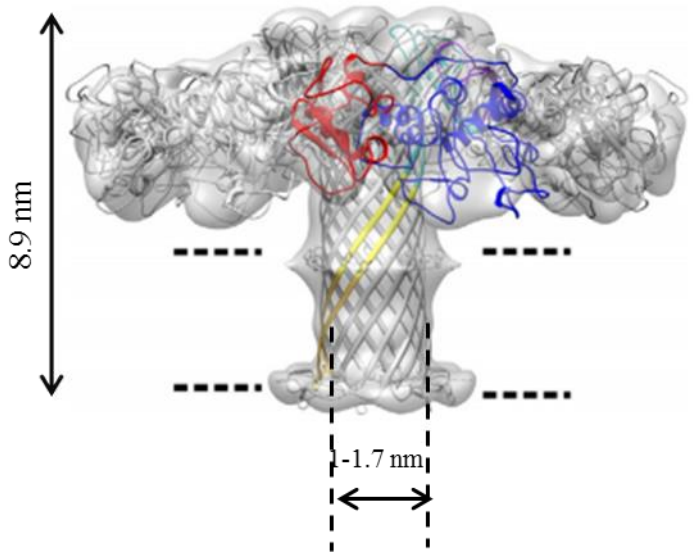

Figure 4. Structure of aerolysin derived from the quasipore map. Aerolysin is a mushroom-shaped β-barrel structure of length ~8.9 nm and has a dimeter of 1 - 1.7 nm. [70]

Biosensing with pore-forming poteins

The stochastic sensing of analytes using nanopores offers great advantages through their versatility and sensitivity. It allows the sensing of molecules like therapeutic agents, toxins, biological weapons and other pollutants [79-81]. Various metal ions such as copper ions, lead, barium, and zinc were detected using an engineered α-HL protein nanopore [20, 81, 82]. The substitution of seven amino acids to create a ring of aromatic amino acids within the lumen of α-HL distinguished 2,4,6-trinitrotoluene from other nitro-aromatics [83], and an engineered α-HL was also shown to detect biologically significant phosphate anions [84]. The incorporation of an adapter like cyclodextrin within the lumen of α-HL enabled the nanopore to sense various organic analytes including antidepressant and antihistaminic drugs [85]. In addition to cyclodextrin, cyclic peptides used as molecular adapters in the β-barrel of α-HL allow it to function as an exquisite sensor for the detection of small polyanions [86]. The attachment of biorecognition elements in the protein nanopore provides another platform

for the use of protein nanopores as biosensors. The attachment of biotin-PEG to the α-HL lumen enabled the detection of streptavidin molecules [87]. Similarly, coupling disaccharide molecules to α-HL allowed for studying the binding kinetics with a ligand lectin, a carbohydrate binding protein from *Bauhinia purpurea* [88]. In line with their outstanding sensing capabilities, nanopores are exploited for early diagnosis and disease management [89]. Biomarkers for lung cancer and human epithelial carcinoma were successfully detected with nanopores at very low concentrations, indicating a tremendous potential for biomedical uses [24, 90].

Biological nanopores as nano-switches for controlled transport

The ability to introduce molecules such as antibodies, drugs, dyes, or therapeutic agents into cells in a non-destructive way is essential for qualitative and quantitative descriptions of fundamental cellular processes and for modulation of crucial functionalities. The loading of bioactive molecules into living cells is challenging due to the selective nature of the plasma-membrane. To overcome the membrane barrier, protein channels are excellent tools with the ability to permeabilize the membrane without destroying the cell. The widely used nanopore α-HL was developed into a metal-actuated nano-switch for controlling the permeabilization of cell membranes [91]. The replacement of five amino-acids with histidines provided α-HL with the additional feature of turning the membrane permeability on/off simply by adding or removing Zn^{2+}. The cholesterol dependent cytolysin streptolysin O, a toxin from streptococci, produces a large pore and is able to deliver cell-impermeant molecules up to 100 kDa in adherent and non-adherent cell lines [92-94]. Listeriolysin-O, a toxin from *Listeria monocytogenes*, is able to efficiently deliver a viral nucleoprotein and a macromolecule antigen to cytotoxic T-lymphocytes

[95-97]. In these studies, listeriolysin O was encapsulated inside liposomes for the efficient cytosolic delivery of molecules. The bacterial mechanosensitive channel MscL from *E. coli* may provide nanoscale pathways for delivering cell-impermeable cargoes into the cytosol without killing the host cells [98]. Moreover, engineered MscL was proposed to be used in artificial membrane systems for drug delivery from pressurized liposomes [99].

Limitations of existing natural nanopores

In spite of their tremendous potential as scientific and engineering tools, nanopores have intrinsic limitations. The small opening of the conducting pathway constitutes a major barrier for larger analytes. The vestibular structures often present in their structure complicate the interaction kinetics and interpretation of experimental data. Not all biological nanopores used for sensing and permeabilization are commercially available, thus on site production and purification may be needed. Insufficient characterization, difficult reconstitution, or poor stability in artificial and natural lipid membranes may significantly restrict their applicability. Also, the lack of intrinsic regulatory mechanisms often hinders their use for controlled transport, and the endowment with such features is not always straightforward. Ideally, a versatile nanopore should be useful for both sensing and controlled transport purposes. To meet this stringent need, we propose using lysenin.

Lysenin as a prototype channel for sensing and controlled permeability

The limitations presented by the biological nanopores used for sensing and permeabilization raises the question about whether a particular wild type protein may constitute a better alternative for the development of nano-tools with a greater

applicability. Along this line, our work focused on investigating lysenin as a transmembrane transporter capable of both stochastic sensing and achievement of controlled membrane permeability. Lysenin is a 297 amino acid protein found in the coelomic fluid of the earthworm *E. fetida* [100-102]. Early studies identified significant cytolytic and hemolytic activities [102-104], as well as a strong ability to disturb smooth muscle contraction [102, 105]. It's lytic activity is selectively restricted to membranes rich in sphingomyelin [100, 101, 104, 106, 107], which is a major component of animal cell plasma lipid membranes. Transmission electron microscopy (TEM) imaging and electrophysiology studies confirmed a lytic mechanism, which relies on lysenin oligomerization into large transmembrane pores inserted into host artificial and natural membranes [14, 108-110]. The complete mechanism of channel formation is yet unknown and currently there is no agreement on the number of monomers required to assemble a functional pore. TEM imaging suggested a hexamer [14] and electron density map a trimer [111], while the most recent structural data points to a nonamer [109]. In spite of such discrepancies, all investigations indicate a large, central large pore of up to ~3 nm in diameter in the center of the oligomerized structure [103, 104, 106, 108].

The recently deciphered lysenin structure (Figure 5) shows a long β-barrel channel of ~11 nm in length and indicates the absence of a vestibule [109, 112]. Lysenin's ability to self-insert large and stable nanopores in artificial membrane systems creates the opportunity to use it as a single molecule sensor in a Coulter setup employing stochastic sensing similar to other biological nanopores. The first attempt to translocate DNA molecules through a single wild-type lysenin channel failed, which was explained by strong electrostatic repulsion between the highly-charged channel domains and the

DNA molecules [109]. The replacement of some negatively-charged amino acids with a combination of neutral and positively charged amino-acids yielded transient changes of the ionic current through single lysenin channels, resembling translocation events [109]. However, no further proof of the translocation of DNA molecules through the recombinant channel was provided.

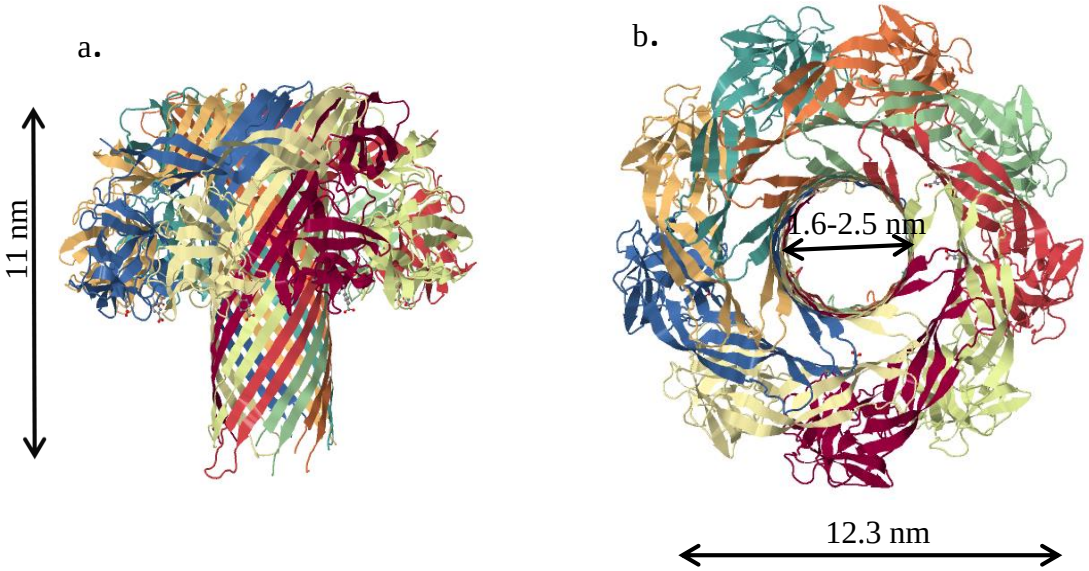

Figure 5. The structure of the lysenin pore. a) Lysenin is a nonameric mushroom shaped β-barrel protein with a length of ~11 nm. b) The top view indicates the nine subunits and a pore size of ~1.6-2.5 nm in diameter. (Adapted from Podobnik et al. (2016), PDB 5EC5 [109])

To demonstrate that wild-type lysenin channels may be used as stochastic sensors, we employed angiotensin II (Ang II) as analyte, which is an octapeptide hormone (Asp-Arg-Val-Tyr-Ile-His-Pro-Phe) that plays a central role in cardiovascular homeostasis [113, 114]. This choice was also motivated by the fact that Ang II bears a fractional positive charge at neutral pH, which may prevent undesired electrostatic repulsions between the cationic peptide and anionic domains present within the channel structure of lysenin [109].

In addition to investigating lysenin channels as single molecule sensors, our efforts expanded into the use of lysenin channels for controlling the permeability of artificial and natural membranes. This component makes exclusive use of lysenin's unique features regarding its transport capabilities. The large conducting pathway ensures a high transport rate, which is common to many PFPs and ion channels. However, unlike many other PFTs, lysenin channels are highly regulated by a multitude of physical and chemical stimuli [115-120], enabling multiple opportunities to achieve controlled transport. The non-symmetrical voltage-induced gating presented by lysenin is not common among PFTs [110, 118, 119]. Many PFTs do present conductance modulation by voltage, however it is symmetric and occurs at unusually large magnitudes of the transmembrane voltage [10]. Lysenin reconstitution into artificial membrane systems at single and multiple channel levels shows a sudden change from a highly-conducting state to a non-conducting state at transmembrane voltages greater than ~15 mV [110, 118]. The open-close transition is presumed to originate in fast conformational changes induced by interactions between the external electric field and a voltage-domain sensor present in the channel's structure [110, 118]. The changes in the conducting state are reversible and the channels re-open after the elimination of the external electric field or through the application of negative bias voltages [110, 118]. Controlled permeabilization via transmembrane voltage manipulation is not so straightforward for live cells, since they present a resting transmembrane potential. Nonetheless, even in living cells, transmembrane potentials may be adjusted by either creating diffusion potentials or by exposing the cells to strong electric fields [121]. Such investigations would benefit significantly if lysenin channels were inserted in and inside-out configuration (i.e., by

microinjection), which would force the lysenin channels into the closed state at physiological transmembrane potentials. Further voltage manipulation may be achieved through membrane polarization under the influence of strong electric fields [121]. Consequently, such manipulations are absolutely feasible in artificial membrane systems for which the transmembrane potential may be varied without affecting the integrity of the system under investigation.

Another feature of lysenin channels, crucial for permeability studies, is their unique regulation by multivalent ions [115-117]. Early studies conducted by our group identified several distinct mechanisms of interaction between lysenin channels and multivalent cations [116, 117]. The exposure of lysenin to sub-mM concentrations of trivalent metal cations such as lanthanides or Al^{3+}, elicited a rapid decrease in the macroscopic conductance, as inferred from the sustained decrease of the ionic current through multiple lysenin channels inserted into planar membranes [116, 117]. Single-channel experiments demonstrate a fast transition between conducting and non-conducting states elicited in the presence of such multivalent metal cations, suggesting a ligand-induced gating mechanism [116, 117]. This essential feature may prove fruitful for exclusive control over membrane permeability by using multivalent cations. In addition, the ligand-induced gating is reversible; the removal of the conductance-inhibiting ions by chelation or precipitation yielded 100% recovery of the membrane conductance, explained by the re-opening observed at single-channel levels [116, 117]. Another important feature of ligand-induced gating is the partial channel closure, manifested in the presence of divalent metal cations or more voluminous, yet multivalent, organic ions [116, 117]. While the resulting sub-conducting states do not completely annihilate the

macroscopic conductance and lysenin-induced permeability, the smaller opening of the conducting pathway may be used for size-selective transport of various molecules across membranes. Also, our recent explorations present reversible channel conductance modulation induced by purines [115], which is detailed in this dissertation.

Permeability control by multivalent ions may constitute an excellent option for artificial membrane systems, which are capable of sustaining the addition of metal ions, chelators, or precipitating agents. However, many of those may prove toxic for living cells, thus restricting their applicability [11]. To avoid such limitations, we used another unique and remarkable feature of lysenin channels, namely irreversible blockage by chitosan [120]. Chitosan is a highly charged linear polysaccharide consisting of N-acetyl-glucosamine and glucosamine with β-1, 4-linkages. It is a product obtained from crustacean shells, and it is considered bio-inert and non-toxic to animals and humans [122, 123]. These life-compatible features support the use of chitosan as an optimal choice for controlling the permeability of live cell membranes in conjunction with lysenin. The two-step process comprising cell permeabilization with lysenin channels followed by chitosan-induced blockage would provide a two-way control over the membrane barrier while preserving cell viability.

Objectives

The major goal of our research was to investigate lysenin channels as both nano-sensors for stochastic sensing and as nano-switches for controlled permeabilization of artificial and natural lipid membranes. To achieve the proposed goal, my work focused on two distinct objectives:

Objective 1: Investigate the translocation of angiotensin II through single lysenin channels inserted into artificial planar lipid membranes

Ang II translocation through single channels inserted into planar lipid membranes was explored through the resistive pulse technique. The transient changes in the ionic current upon peptide-channel interactions were analyzed with specialized software to determine amplitude and dwell time. The influence of applied voltage on the electronic signature, in conjunction with previous interpretations on macromolecule-channel interactions, enabled discrimination between putative translocations and channel-peptide collisions. The density plot of recorded events identified an excellent translocation/collision separation, which is unmatched in translocation experiments employing other channels and short peptides. Separate experiments that employed large populations of lysenin channels and extended time allowed mass spectrometry and liquid chromatography identification of electrophoretically-driven peptide translocation only through un-blocked lysenin channels.

Objective 2. Exploit lysenin regulatory properties for controlling the permeability of artificial and natural membrane systems

The ability to control the membrane permeability was tested in artificial membrane systems (bilayer membranes and liposomes) and in the plasma membrane of live cells (Jurkat and ATDC5). Our explorations indicated that ATP may be used to reversibly modulate the macroscopic ionic conductance of lysenin channels in single and multiple channel experiments. Next, assessments enabled the analysis of diffusive transport of membrane impermeable calcein dye into lysenin-permeabilized liposome membranes. The addition of multivalent Al^{3+} cations induced simultaneous channel

blockage and quenching of non-entrapped calcein, which facilitated microscopy imaging. In addition, multivalent metal cation removal by precipitation reverted the membrane to a highly permeable state and initiated calcein leakage into the bulk solution. Further experiments on lysenin-induced live cell permeabilization employed non-permeant dyes, dead/live dye indicators, and lysenin channels blockage by chitosan. Separate electrophysiology investigations were aimed at deciphering lysenin's potential interactions with dyes in order to eliminate any undesired interference with the biological system under consideration. Permeability and viability estimations were employed using confocal microscopy and fluorescence spectroscopy as major techniques for qualitative and quantitative assessments.

References

1. Aldrich, R.W., *Voltage-dependent gating of sodium channels: towards an integrated approach.* Trends in Neuro Sciences, 1986. **9**(2): p. 82-86.

2. Bezanilla, F., *Voltage-gated ion channels.* IEEE Transactions on Nanobioscience, 2005. **4**(1): p. 34-48.

3. Hille, B., *Ion channels of exctable membranes, Third edition*. 2001, Sunderland, MA: Sinauer Associates, Inc.

4. Saier, M.H.J., *Families of transporters and their classification*, in *Transmembrane Transporters*, M.W. Quick, Editor. 2002, Wiley-Liss, Inc.: New Jersey. p. 1-17.

5. Sigworth, F.J., *Voltage gating of ion channels.* Quarterly Reviews of Biophysics, 1994. **27**: p. 1-40.

6. Swartz, K.J., *Sensing voltage across lipid membranes.* Nature, 2008. **456**(18): p. 891-897.

7. Aidley, D.J. and P.R. Stanfield, *Ion Channels. molecules in action*. 1996, Cambridge: Cambridge University Press.

8. Andersen, O.S., H.I. Ingolfsson, and J.A. Lundbaek, *Ion channels.* Wiley Encyclopedia of Chemical Biology, 2008: p. 1-14.

9. Ashcroft, F.M., *Ion channels and disease*. 1999, San Diego, CA, USA: Academic Press.

10. Bainbridge, G., I. Gokce, and J.H. Lakey, *Voltage gating is a fundamental feature of porin and toxin β-barrel membrane channels.* FEBS letters, 1998. **431**(3): p. 305-308.

11. Bashford, C.L., *Pore-forming toxins: attack and defense at the cell surface.* Cellular & Molecular Biology Letters, 2001. **6**(2A): p. 328-333.

12. Leippe, M., *Pore-forming toxins from pathogenic amoebae.* Applied Microbiology and Biotechnology, 2014. **98**(10): p. 4347-4353.

13. Sher, D., et al., *Hydralysins, a new category of beta-pore-forming toxins in cnidaria.* Journal of Biological Chemistry, 2005. **280**(24): p. 22847-22855.

14. Shogomori, H. and T. Kobayashi, *Lysenin: A sphingomyelin specific pore-forming toxin.* Biochimica et Biophysica Acta, 2008. **1780**(3): p. 612-618.

15. Anderluh, G., et al., *Cysteine-scanning mutagenesis of an eukaryotic pore-forming toxin from sea anemone: topology in lipid membranes.* European Journal of Biochemistry, 1999. **263**(1): p. 128-136.

16. Fontes, W., et al., *Determination of the amino acid sequence of the plant cytolysin enterolobin.* Archives of Biochemistry Biophysics, 1997. **347**(2): p. 201-207.

17. Sousa, M.V., et al., *Homology between the seed cytolysin enterolobin and bacterial aerolysins.* Journal of Protein Chemistry, 1994. **13**(8): p. 659-667.

18. Mariani, E., et al., *Perforins in human cytolytic cells: the effect of age.* Mechanism of Ageing Development, 1996. **92**(2-3): p. 195-209.

19. Bayley, H., *Nanopore sequencing: from imagination to reality*. Clinical chemistry, 2015. **61**(1): p. 25-31.

20. Wang, G., et al., *Nanopore detection of copper ions using a polyhistidine probe.* Biosensors and Bioelectronics, 2014. **53**: p. 453-458. doi: 10.1016/j.bios.2013.10.013

21. Li, J., et al., *Characterization of protein unfolding with solid-state nanopores.* Protein and peptide letters, 2014. **21**(3): p. 256-265.

22. Laszlo, A.H., et al., *Decoding long nanopore sequencing reads of natural DNA.* Nature Biotechnology, 2014. **32**(8): p. 829-833.

23. Ying, Y.-L., et al., *A stimuli-responsive nanopore based on a photoresponsive host-guest system.* Scientific Reports, 2013. **3**. doi: 10.1038/srep01662

24. Wang, S., et al., *Engineered nanopore of Phi29 DNA-packaging motor for real-time detection of single colon cancer specific antibody in serum.* ACS Nano, 2013. **7**(11): p. 9814-9822.

25. Mura, S., J. Nicolas, and P. Couvreur, *Stimuli-responsive nanocarriers for drug delivery.* Nature Materials, 2013. **12**(11): p. 991-1003.

26. Laszlo, A.H., et al., *Detection and mapping of 5-methylcytosine and 5-hydroxymethylcytosine with nanopore MspA.* Proceedings of the National Academy of Sciences, 2013. **110**(47): p. 18904-18909.

27. Wanunu, M., *Nanopores: A journey towards DNA sequencing.* Physics of life reviews, 2012. **9**(2): p. 125-158.

28. Coulter, W.H., *Means for counting particles suspended in a fluid*. 1953: US.

29. Li, J., et al., *DNA molecules and configurations in a solid-state nanopore microscope.* Nature Materials, 2003. **2**: p. 611-615. doi: 10.1038/nmat965

30. Kasianowicz, J.J., et al., *Characterization of individual polynucleotide molecules using a membrane channel.* Proceedings of the National Academy of Sciences , 1996. **93**(24): p. 13770-13773.

31. Akeson, M., et al., *Microsecond time-scale discrimination among polycytidylic acid, polyadenylic acid, and polyuridylic acid as homopolymers or as segments within single RNA molecules.* Biophysical Journal, 1999. **77**(6): p. 3227-3233.

32. Meller, A., *Dynamics of polynucleotide transport through nanometre-scale pores.* Journal of Physics: Condensed Matter, 2003. **15**(17): p. R581-R607.

33. Aksimentiev, A., et al., *Microscopic kinetics of DNA translocation through synthetic nanopores.* Biophysical Journal, 2004. **87**(3): p. 2086-2097.

34. Mathé, J., et al., *Orientation discrimination of single-stranded DNA inside the alpha-hemolysin membrane channel.* Proceedings of the National Academy of Sciences , 2005. **102**(35): p. 12377-12382.

35. Fologea, D., et al., *Detecting single stranded DNA with a solid state nanopore.* Nano Letters, 2005. **5**(10): p. 1905-1909.

36. Fologea, D., et al., *Slowing DNA translocation in a solid state nanopore.* Nano Letters, 2005. **5**(9): p. 1734-1737.

37. Fologea, D., et al., *DNA conformation and base number simultaneously determined in a nanopore.* Electrophoresis, 2007. **28**(18): p. 3186-3192.

38. Mihovilovic, M., N. Hagerty, and D. Stein, *Statistics of DNA capture by a solid-state nanopore.* Physical Review Letters, 2013. **110**(2): p. 028102. doi: 10.1103/PhysRevLett.110.028102

39. Majd, S., et al., *Applications of biological pores in nanomedicine, sensing, and nanoelectronics.* Current Opinion in Biotechnology, 2010. **21**(4): p. 439-476.

40. Song, L., et al., *Structure of staphylococcal alpha-hemolysin, a heptameric transmembrane pore.* Science, 1996. **274**(5294): p. 1859-1866.

41. Meller, A., et al., *Rapid nanopore discrimination between single polynucleotide molecules.* Proceedings of the National Academy of Sciences, 2000. **97**(3): p. 1079-1084.

42. Mitchell, N. and S. Howorka, *Chemical tags facilitate the sensing of individual DNA strands with nanopores.* Angewandte Chemie International Edition, 2008. **47**(30): p. 5565-5568.

43. Stoddart, D., et al., *Single-nucleotide discrimination in immobilized DNA oligonucleotides with a biological nanopore.* Proceedings of the National Academy of Sciences, 2009. **106**(19): p. 7702-7707.

44. Stoddart, D., et al., *Nucleobase recognition in ssDNA at the central constriction of the alpha-hemolysin pore.* Nano Letters, 2010. **10**(9): p. 3633-3637.

45. Fuller, C.W., et al., *Real-time single-molecule electronic DNA sequencing by synthesis using polymer-tagged nucleotides on a nanopore array.* Proceedings of the National Academy of Sciences, 2016. **113**(19): p. 5233-5238.

46. Kumar, S., et al., *PEG-labeled nucleotides and nanopore detection for single molecule DNA sequencing by synthesis.* Scientific Reports, 2012. **2**. doi: 10.1038/srep00684

47. Clarke, J., et al., *Continuous base identification for single-molecule nanopore DNA sequencing.* Nature Nanotechnology, 2009. **4**(4): p. 265-267.

48. Lu, H., F. Giordano, and Z. Ning, *Oxford Nanopore MinION Sequencing and Genome Assembly.* Genomics Proteomics Bioinformatics, 2016. **14**(5): p. 265-279.

49. Faller, M., M. Niederweis, and G.E. Schulz, *The structure of a mycobacterial outer-membrane channel.* Science, 2004. **303**(5661): p. 1189-1192.

50. Butler, T.Z., et al., *Single-molecule DNA detection with an engineered MspA protein nanopore.* Proceedings of the National Academy of Sciences, 2008. **105**(52): p. 20647-20652.

51. Manrao, E.A., et al., *Nucleotide discrimination with DNA immobilized in the MspA nanopore.* PLoS One, 2011. **6**(10): p. e25723. doi: 10.1371/journal.pone.0025723

52. Derrington, I.M., et al., *Nanopore DNA sequencing with MspA.* Proceedings of the National Academy of Sciences, 2010. **107**(37): p. 16060-16065.

53. Manrao, E.A., et al., *Reading DNA at single-nucleotide resolution with a mutant MspA nanopore and phi29 DNA polymerase.* Nature Biotechnology, 2012. **30**(4): p. 349-353.

54. Robertson, J.W., et al., *Single-molecule mass spectrometry in solution using a solitary nanopore.* Proceedings of the National Academy of Sciences, 2007. **104**(20): p. 8207-8211.

55. Reiner, J.E., et al., *Theory for polymer analysis using nanopore-based single-molecule mass spectrometry.* Proceedings of the National Academy of Sciences, 2010. **107**(27): p. 12080-12085.

56. Wallace, E.V.B., et al., *Identification of epigenetic DNA modifications with a protein nanopore.* Chemical Communications, 2010. **46**(43): p. 8195-8197.

57. Zhang, X., et al., *Characterization of Interstrand DNA-DNA Cross-Links Using the α-Hemolysin Protein Nanopore.* ACS Nano, 2015. **9**(12): p. 11812-11819.

58. Jin, Q., et al., *Unzipping kinetics of duplex DNA containing oxidized lesions in an α-hemolysin nanopore.* Journal of American Chemical Society, 2012. **134**(26): p. 11006-11011.

59. Johnson, R.P., et al., *Base flipping within the α-hemolysin latch allows single-molecule identification of mismatches in DNA.* Journal of American Chemical Society, 2016. **138**(2): p. 594-603.

60. Zeng, T., et al., *Interrogation of base pairing of the spiroiminodihydantoin diastereomers using the α-hemolysin latch.* Biochemistry, 2017. **56**(11): p. 1596-1603.

61. Movileanu, L., et al., *Interactions of peptides with a protein pore.* Biophysical Journal, 2005. **89**(2): p. 1030-1045.

62. Stefureac, R., et al., *Transport of a-helical peptides through a-hemolysin and aerolysin pores.* Biochemistry, 2006. **45**(30): p. 9172-9179.

63. Zhao, Q., et al., *Study of peptide transport through engineered protein channels.* The Journal of Physical Chemistry B, 2009. **113**(11): p. 3572-3578.

64. Wolfe, A.J., et al., *Catalyzing the translocation of polypeptides through attractive interactions.* Journal of American Chemical Society, 2007. **129**(45): p. 14034-14041.

65. Oukhaled, G., et al., *Unfolding of proteins and long transient conformations detected by single nanopore recording.* Physical Review Letters, 2007. **98**(15): p. 158101. doi: 10.1103/PhysRevLett.98.158101

66. Goodrich, C.P., et al., *Single-molecule electrophoresis of beta-hairpin peptides by electrical recordings and Langevin dynamics simulations.* The Journal of Physical Chemistry B, 2007. **111**(13): p. 3332-3335.

67. Nivala, J., D.B. Marks, and M. Akeson, *Unfoldase-mediated protein translocation through an [alpha]-hemolysin nanopore.* Nature Biotechnology, 2013. **31**(3): p. 247-250.

68. Parker, M.W., et al., *Structure of the Aeromonas toxin proaerolysin in its water-soluble and membrane-channel states.* Nature, 1994. **367**(6460): p. 292-295.

69. Tsitrin, Y., et al., *Conversion of a transmembrane to a water-soluble protein complex by a single point mutation.* Nature Structural and Molecular Biology, 2002. **9**(10): p. 729-733.

70. Iacovache, I., et al., *Cryo-EM structure of aerolysin variants reveals a novel protein fold and the pore-formation process.* Nature Communications, 2016. **7**. doi: 10.1038/ncomms12062

71. Cao, C., et al., *Discrimination of oligonucleotides of different lengths with a wild-type aerolysin nanopore.* Nature Nanotechnology, 2016. **11**(8): p. 713-718.

72. Cao, C., et al., *Driven Translocation of polynucleotides through an aerolysin Nanopore.* Anaytical Chemistry, 2016. **88**(10): p. 5046-5049.

73. Pastoriza-Gallego, M., et al., *Evidence of unfolded protein translocation through a protein nanopore.* ACS nano, 2014. **8**(11): p. 11350-11360.

74. Pastoriza-Gallego, M., et al., *Dynamics of unfolded protein transport through an aerolysin pore.* Journal of the American Chemical Society, 2011. **133**(9): p. 2923-2931.

75. Payet, L., et al., *Thermal unfolding of proteins probed at the single molecule level using nanopores.* Analytical Chemistry, 2012. **84**(9): p. 4071-4076.

76. Merstorf, C., et al., *Wild type, mutant protein unfolding and phase transition detected by single-nanopore recording.* ACS Chemical Biology, 2012. **7**(4): p. 652-658.

77. Fennouri, A., et al., *Single molecule detection of glycosaminoglycan hyaluronic acid oligosaccharides and depolymerization enzyme activity using a protein nanopore.* ACS Nano, 2012. **6**(11): p. 9672-9678.

78. Fennouri, A., et al., *Kinetics of enzymatic degradation of high molecular weight polysaccharides through a nanopore: experiments and data-modeling.* Analytical Chemistry, 2013. **85**(18): p. 8488-8492.

79. Bayley, H. and P.S. Cremer, *Stochastic sensors inspired by biology.* Nature, 2001. **413**(6852): p. 226-230.

80. Bayley, H. and C.R. Martin, *Resistive-pulse sensing from microbes to molecules.* Chemical Reviews, 2000. **100**(7): p. 2575-2594.

81. Braha, O., et al., *Designed protein pores as components for biosensors.* Chemistry & Biology, 1997. **4**(7): p. 497-505.

82. Yang, C., et al., *Highly sensitive simultaneous detection of lead (ii) and barium (ii) with g-quadruplex DNA in alpha-hemolysin nanopore.* Analytical Chemistry, 2013. **85**(15): p. 7302-7307.

83. Guan, X., et al., *Stochastic sensing of TNT with a genetically engineered pore.* Chembiochem, 2005. **6**(10): p. 1875-1881.

84. Cheley, S., L.Q. Gu, and H. Bayley, *Stochastic sensing of nanomolar inositol 1,4,5-trisphosphate with an engineered pore.* Chemistry and Biology, 2002. **9**(7): p. 829-838.

85. Gu, L.Q., et al., *Stochastic sensing of organic analytes by a pore-forming protein containing a molecular adapter.* Nature, 1999. **398**(6729): p. 686-690.

86. Sanchez-Quesada, J., et al., *Cyclic peptides as molecular adapters for a pore-forming protein*. Journal of the American Chemical Society, 2000. **122**(48):p1157-11766

87. Movileanu, L., et al., *Detecting protein analytes that modulate transmembrane movement of a polymer chain within a single protein pore.* Nature Biotechnology, 2000. **18**(10): p. 1091-1095.

88. Howorka, S., et al., *Stochastic detection of monovalent and bivalent protein-ligand interactions.* Angewandte Chemie International Edition, 2004. **43**(7): p. 842-846.

89. Reiner, J.E., et al., *Disease detection and management via single nanopore-based sensors.* Chemical Reviews, 2012. **112**(12): p. 6431-6451.

90. Wang, Y., et al., *Nanopore-based detection of circulating microRNAs in lung cancer patients.* Nature Nanotechnology, 2011. **6**(10): p. 668-674.

91. Russo, M.J., H. Bayley, and M. Toner, *Reversible permeabilization of plasma membranes with an engineered switchable pore.* Nature Biotechnology, 1997. **15**(3): p. 278-282.

92. Walev, I., et al., *Delivery of proteins into living cells by reversible membrane permeabilization with streptolysin-O.* Proceedings of the National Academy of Sciences, 2001. **98**(6): p. 3185-3190.

93. Spiller, D.G. and D.M. Tidd, *Nuclear delivery of antisense oligodeoxynucleotides through reversible permeabilization of human leukemia cells with streptolysin O.* Antisense Research and Development, 1995. **5**(1): p. 13-21.

94. Teng, K.W., et al., *Labeling proteins inside living cells using external fluorophores for fluorescence microscopy.* Elife, 2017. **6**: p. e25460. doi: 10.7554/eLife.20378

95. Mandal, M. and K.D. Lee. *Listeriolysin O-containing-liposome mediated cytosolic delivery of exogenous antigen*. in *FASEB JOURNAL*. 2000.

96. Mandal, M. and K.D. Lee, *Listeriolysin O-liposome-mediated cytosolic delivery of macromolecule antigen in vivo: enhancement of antigen-specific cytotoxic T lymphocyte frequency, activity, and tumor protection.* Biochimica et Biophysica Acta-Biomembranes, 2002. **1563**(1-2): p. 7-17.

97. Mandal, M., et al., *Cytosolic delivery of viral nucleoprotein by listeriolysin O-liposome induces enhanced specific cytotoxic T lymphocyte response and protective immunity.* Molecular pharmaceutics, 2004. **1**(1): p. 2-8.

98. Doerner, J.F., S. Febvay, and D.E. Clapham, *Controlled delivery of bioactive molecules into live cells using the bacterial mechanosensitive channel MscL.* Nature Communications, 2012. **3**: p. 990. doi: 10.1038/ncomms1999

99. Louhivuori, M., et al., *Release of content through mechano-sensitive gates in pressurized liposomes.* Proceedings of the National Academy of Sciences, 2010. **107**(46): p. 19856-19860.

100. Shakor, A.-B.A., E.A. Czurylo, and A. Sobota, *Lysenin, a unique sphingomyelin-binding protein.* FEBS Letters, 2003. **542**: p. 1-6.

101. Kiyokawa, E., et al., *Recognition of sphingomyelin by lysenin and lysenin-related proteins.* Biochemistry, 2004. **43**(30): p. 9766-9773.

102. Kobayashi, H., N. Ohta, and U. Masato, *Biology of lysenin, a protein in the coelomic fluid of the earthworm Eisenia foetida.* International Review of Cytology, 2004. **236**: p. 45-99.

103. Bruhn, H., et al., *Dissection of the mechanisms of cytolytic and antibacterial activity of lysenin, a defence protein of the annelid Eisenia fetida.* Developmental and Comparative Immunology, 2006. **30**(7): p. 597-606.

104. Yamaji-Hasegawa, A., et al., *Oligomerization and pore formation of a sphingomyelin-specific toxin, lysenin.* The Journal of Biological Chemistry, 2003. **278**(25): p. 22762-22770.

105. Czurylo, E.A., N. Kulikova, and A. Sobota, *Disturbance of smooth muscle regulatory function by Eisenia foetida toxin lysenin: Insight into the mechanism of smooth muscle contraction.* Toxicon, 2008. **51**(6): p. 1090-1102.

106. Ishitsuka, R. and T. Kobayashi, *Lysenin: A new tool for investigating membrane lipid organization.* Anatomical Science International, 2004. **79**(4): p. 184-190.

107. Yamaji, A., et al., *Lysenin, A novel sphingomyelin-specific binding protein.* The Journal of Biological Chemistry, 1998. **273**(9): p. 5300-5306.

108. Kwiatkowska, K., et al., *Lysenin-His, a sphingomyelin-recognizing toxin, requires tryptophan 20 for cation-selective channel assembly but not for membrane binding.* Molecular Membrane Biology, 2007. **24**(2): p. 121-134.

109. Podobnik, M., et al., *Crystal structure of an invertebrate cytolysin pore reveals unique properties and mechanism of assembly.* Nature Communications, 2016. **7.** doi: 10.1038/ncomms11598

110. Ide, T., et al., *Lysenin forms a voltage-dependent channel in artificial lipid bilayer membranes.* Biochemical and Biophysical Research Communications, 2006. **346**(1): p. 288-292.

111. De Colibus, L., et al., *Structures of lysenin reveal a shared evolutionary origin for pore-forming proteins and its mode of sphingomyelin recognition.* Structure, 2012. **20**(9): p. 1498-1507.

112. Bokori-Brown, M., et al., *Cryo-EM structure of lysenin pore elucidates membrane insertion by an aerolysin family protein.* Nature Communications, 2016. **7**. doi: 10.1038/ncomms11293

113. De Mello, W.C. and A.H.J. Danser, *Angiotensin II and the heart.* Hypertension, 2000. **35**(6): p. 1183-1188.

114. Taubman, M.B., *Angiotensin II.* Circulation Research, 2003. **92**(1): p. 9-11.

115. Bryant, S., et al., *Purinergic control of lysenin's transport and voltage-gating properties.* Purinergic Signal, 2016.**12**(3): p. 549-559

116. Fologea, D., et al., *Potential analytical applications of lysenin channels for detection of multivalent ions.* Analytical Bioanalytical Chemistry, 2011. **401**(6): p. 1871-1879.

117. Fologea, D., et al., *Multivalent ions control the transport through lysenin channels.* Biophysical Chemistry, 2010. **152**(1-3): p. 40-45.

118. Fologea, D., et al., *Controlled gating of lysenin pores.* Biophysical Chemistry, 2010. **146**(1): p. 25-29.

119. Fologea, D., et al., *Bi-stability, hysteresis, and memory of voltage-gated lysenin channels.* Biochimica et Biophysica Acta, Biomembranes, 2011. **1808**(12): p. 2933-2939.

120. Fologea, D., et al., *Cationic polymers inhibit the conductance of lysenin channels.* The Scientific World Journal, 2013**.** doi: 10.1155/2013/316758

121. Jordan, C.A., E. Neumann, and A.E. Sowers, *Electroporation and electrofusion in cell biology*. 1989: Springer US.

122. Aspden, T.J., et al., *Chitosan as a nasal delivery system: the effect of chitosan solutions on in vitro and in vivo mucociliary transport rates in human turbinates and volunteers.* Journal of Pharmaceutical Sciences, 1997. **86**(4): p. 509-513.

123. Rao, S.B. and C.P. Sharma, *Use of chitosan as a biomaterial: studies on its safety and hemostatic potential.* Journal of Biomedical Materials Research, 1997. **34**(1): p. 21-28.

CHAPTER TWO: TRANSLOCATION OF ANGIOTENSIN II THROUGH LYSENIN CHANNELS

Abstract

Here we show that single wild-type lysenin channels inserted into artificial lipid membranes may function as stochastic sensors for peptide molecules by using the resistive-pulse technique. The interactions between angiotensin II and single lysenin channels inserted into planar bilayer lipid membranes yielded transient changes in the ionic open current established through the channel's conducting pathway. Further analysis of the recorded transient events, in terms of current blockage and dwell time allowed us to identify two distinct classes of events. These events were classified either as putative translocations or collisions. To aid data interpretation, we analyzed the influence of applied voltage on both current blockage and dwell time distribution characteristic to each event class. To irrefutably demonstrate that angiotensin II molecules cross the membrane through open lysenin nanopores, we performed extended experiments comprising thousands of inserted channels together with qualitative and quantitative analysis by employing liquid chromatography – mass spectroscopy. The translocated molecules were detected only when the membrane contained lysenin channels in the open state and the electric field had such an orientation to electrophoretically drive the peptides towards the membrane. Taken together, our studies demonstrate that un-modified lysenin channels may be used for stochastic sensing of

macromolecules, which may open novel avenues for single molecule detection and characterization, biosensing, early diagnosis, and sequencing.

Introduction

The ultra-small ionic currents established through a biological or synthetic channel embedded into an otherwise insulating membrane may suffer minuscule yet measurable changes upon interactions between the nanopore and molecules in solution [1-4]. This broad measuring principle emerged into numerous nanopore-based technologies intended to revolutionize science, technology and medicine by utilizing the ultimate sensitivity at the molecular or sub-molecular scale. More than two decades ago, Kasianowicz *et al*. demonstrated that polynucleotides may translocate through alpha-hemolysin (α-HL) nanopores reconstituted into artificial bilayer lipid membranes (BLMs) [1]. This early work employed the resistive pulse technique in which a voltage-clamp setup is used to measure changes in ionic currents when molecules are passing through single channels [1]. At this early inception, the ambitious idea of using nanopores for fast, cheap and reliable DNA sequencing emerged, which started a scientific and technological race around the world. DNA sequencing, the big prize of the race, received the most attention from scientists who engaged in numerous experimental and theoretical explorations on nanopore sequencing. Novel synthetic and biological nanopores have been exploited as candidates for sequencing, and multiple measuring principles have been proposed [4-11]. As a result of the rapid advancement in this field, Oxford Nanopore Technology, in 2014, launched the MinION Access Program, providing early access to the first portable nanopore-based sequencer, and several studies reported accurate readings of increased DNA length [12-18].

However, in depth explorations of nanopore-based technologies are more and more focused on detection, identification, and characterization of proteins and their interaction [7, 19-23]. Peptides and proteins hold a significant importance in living organisms as they play critical roles in the onset of cancer, neurodegenerative disorders, and infections [24-26], and often their expression levels correlate with disease [27-29]. Several studies have explored natural nanopores for peptide and protein sensing including α-HL, aerolysin, phi29 connector channel, and ClyA [9, 19, 30-34]. However, α-HL and aerolysin, both have a narrow size constriction of ~1.4 nm which limits their applicability for structural analysis of peptides. The viral phi29 DNA packaging system has a wider diameter of 3.6 - 6 nm, which is able to translocate double-stranded DNA, but needs to be first reconstituted into liposomes and then incorporated into the lipid planar bilayer membrane, making the process tedious [8]. The larger protein channel, ClyA is able to translocate and detect folded proteins, but this nanopore exists in different oligomeric states and requires further purification before use [32, 33]. Synthetic nanopores are scalable, chemically and mechanically robust, but their production may not ensure a high geometric repeatability [35-37]. Biological nanopores offer unsurpassed structural and dimensional repeatability, and often their sensing capabilities may be tailored by chemical modifications or bio-engineering [9, 38-40]. In the pursuit of finding novel, efficient and better nanopores, we propose lysenin as a new sensing tool for nanopore-based technologies.

Lysenin is a nonameric pore-forming toxin extracted from the coelomic fluid of the earthworm *E. foetida* which self-inserts into the BLMs containing sphingomyelin [41, 42, 43]. Recent studies show that the lysenin channel is a long β-barrel of ~9 -11 nm with

a large pore diameter (~2.5 nm) [41, 42]. In contrast to other pore-forming toxins, lysenin is regulated by voltage, ligands, and polymeric cations [44-49]. Owing to its large conductance and outstanding stability when reconstituted into artificial lipid membranes, we hypothesized that lysenin is an exceptional candidate for analysis and characterizations of single macromolecule by using the resistive pulse technique. In the present study, we employed electrophysiology techniques to investigate the interactions between angiotensin II, an important cardiovascular peptide and single lysenin channels inserted into planar membranes. The translocation of peptides was confirmed by liquid chromatography-mass spectroscopy (LC-MS) analysis of the analyte electrophoretically driven through large populations of lysenin channels.

Materials and Methods

Preparation of bilayer lipid membrane and single channel insertion

A classic BLM setup was used for membrane preparation, channels insertion, and peptide translocation experiments [49-51]. The bilayer chamber (Figure 1) consisted of two ~1 ml reservoirs made out of polytetrafluoroethylene (PTFE) and separated by a thin PTFE film (120 μm thickness). The film was pierced by a high-voltage electric spark and the resulting hole (~60 μm diameter) was painted with less than 1 μl lipid mixture containing diphytanoyl phosphatidylcholine (Avanti Polar Lipids), sphingomyelin (Avanti Polar Lipids), and cholesterol (Sigma-Aldrich), weight ratio 4:2:2, and dissolved in n-decane. The use of neutral lipids was justified by the need to maximize suppression of the voltage induced gating that manifests at positive potentials for lysenin channels inserted into charged membranes [46, 49]. The two reservoirs were filled with 1M KCl buffered with 10 mM Tris and 1 mM EDTA (pH 6.9). Two Ag/AgCl electrodes

immersed into the electrolyte solutions on each side of the membrane were used for electrical connections to the Axopatch 200B amplifier (Molecular Devices) set in the voltage-clamp mode. The analog signal from the amplifier was fed into the Digidata 1440A Digitizer (Molecular Devices) for online visualization and digital recording with the Clampex 10.5.2.6 software package (Molecular Devices). The lipid membrane formation was monitored by capacitance measurement, and the bilayer integrity was checked by measuring the seal resistance at 100 mV bias potential. For a 60 μm hole in the PTFE film, a good bilayer was confirmed by measuring a capacitance larger than 65 pF and a seal resistance greater than 500 GΩ.

After the bilayer membrane formation, single channel experiments comprised of channel self-insertion by the addition of 1 μl of 100 nM lysenin solution (Sigma-Aldrich) to the *cis* (ground) reservoir. Continuous mixing of the electrolyte solution during insertion at -60 mV bias potential was performed with a low noise Bilayer Magnetic Stirrer (Warner Instruments). To prevent further insertions, after reconstitution of one or few lysenin channels in the membrane, the reservoir was flushed with 30 ml of lysenin-free buffered electrolyte solution.

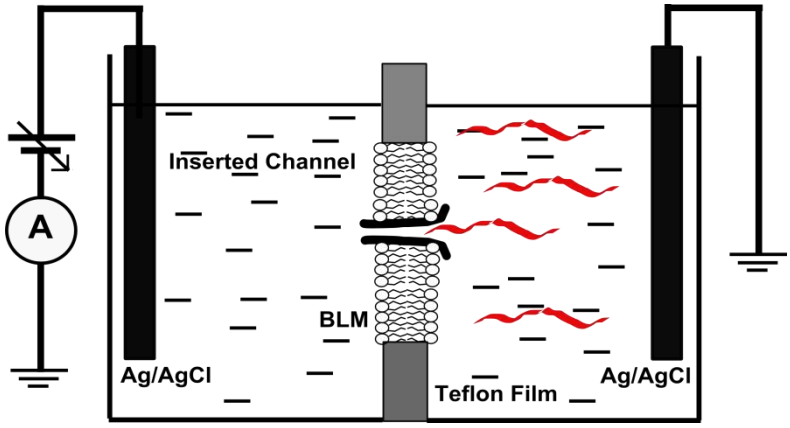

Figure 1. The experimental setup for Ang II translocation employs single lysenin channels inserted into planar bilayer lipid membranes.

Translocation of angiotensin II through single lysenin channels inserted into lipid membranes

Ang II was added at a final concentration of 1 μg mL^{-1} into the appropriate reservoir and the solutions stirred for ~ 10 seconds at maximum speed to ensure uniform mixing. Data recording was performed in dual-channel mode by using the variable-length protocol at a sampling rate of 250 ksample/s, 10 kHz hardware filter, and 1ms post- and pre-trigger length. Digital data saved in the *abf* format have been further analyzed with Clampfit 10.2 (Molecular Devices), Transalyzer [52], Matlab (Mathworks), and Origin 8.5 (OriginLab Corporation) software packages. The Transalyzer package was set to calculate the dwell time as the Full Width Half Maximum for each individual event. The average level between the first and the last local minima of each event selected for analysis was used to compute the current blockage [52].

Insertion of large populations of lysenin channels into membranes

An experimental protocol similar to that for single channels was employed for insertion of multiple channels into the bilayer membrane. To accommodate a larger number of channels, the diameter of the hole in the PTFE film was increased to ~180 μm

by applying multiple electric sparks to a film pre-drilled with a thin needle. The volume of the electrolyte reservoir was lowered to 100 µl and a higher amount of lysenin was added to the *cis* reservoir for insertion. The number of channels residing in the membrane was estimated from the slope of the I-V curve recorded for a narrow voltage range (Figure 2) and by accounting for the individual channel conductance (which is ~ 2.03 nS in otherwise identical experimental conditions). Multiple channel experiments comprised ~ 22,700 channels; when required, the number of the inserted channels was up-adjusted by successive addition of lysenin to the electrolyte solutions.

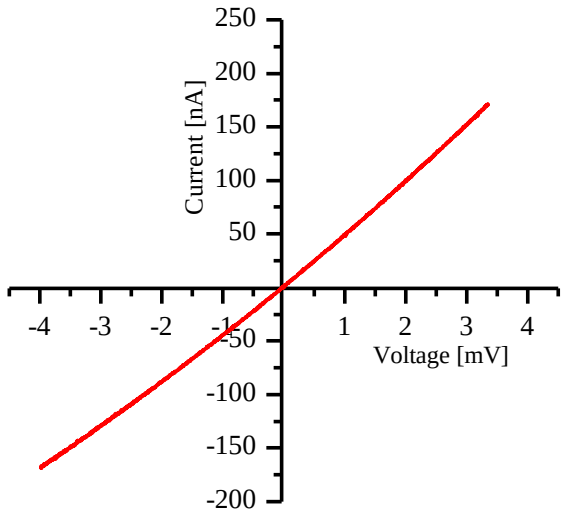

Figure 2. The I-V plot obtained after the insertion of large populations of lysenin channels into BLM. The slope of the curve was calculated to determine the macroscopic conductance and hence the number of channels inserted to the membrane. (Adapted from Shrestha et al. (2017) [53])

Ang II translocation through large populations of lysenin channels comprised addition of 10 µg peptide to the *cis* reservoir while biasing the membrane by -100 mV for ~36 hours. To avoid evaporation, both reservoirs were covered with small pieces of parafilm or silicone films. Each bilayer was checked for integrity at the end of

experiments and the failed ones discarded from analysis. One control experiment employed membranes biased by opposite voltages (+100 mV, to electrophoretically drive the peptide away from the membrane). The second control comprised irreversible blockage of lysenin channels by *cis* addition of 5 µL of 0.1% (m/v) chitosan solubilized in 0.1M acetic acid. The addition of this strong inhibitor of lysenin's conductance [54] yielded a rapid decrease of the ionic current (Figure 3), hence indicating channel blockage. Next, Ang II was added to the ground reservoir, both reservoirs were covered to prevent evaporation, and the membranes biased by -100 mV for 36 hours.

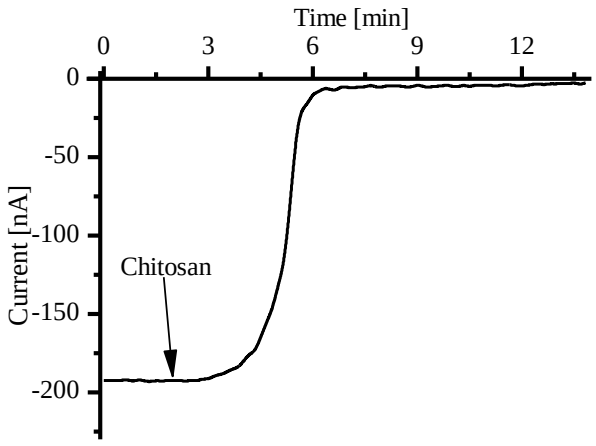

Figure 3. Chitosan addition induced a sustained and irreversible decrease of the macroscopic conductance, indicative of channel blockage. (Adapted from Shrestha et al. (2017) [53])

Liquid chromatography-mass spectroscopy analysis of angiotensin II translocated through large populations of lysenin channels

Translocated samples from the *trans* reservoir were carefully collected after running the experiment for extensive time without disturbing the lipid membrane. The samples were analyzed using Bruker maXis quadrupole-time-of-flight (Q-TOF) mass spectrometer with an electrospray ionization (ESI) Source (Bruker Daltonics). A Dionex

Ultimate 3000 LC system (Dionex) was attached with ESI-Q-TOF. Samples placed in an autosampler at 4°C were injected into C18 column (150 x 2.1 mm, 4 µm, Phenomenex) and the temperature was maintained at 40 °C for chromatographic separation. The elution mobile phases for LC comprised of 5% acetonitrile with 0.1% formic acid (solvent A) and pure acetonitrile with 0.1% formic acid (solvent B). The LC flow rate was kept at 200 µl/min and the elution began with 0% B for 9 mins, 25% B for over 10 mins, 60% B for over 11 mins, and held at this percentage for additional 21 mins. Mass spectrometry was achieved in positive ion mode with a spray voltage of 3000 V with an endplate offset at -500 V, dry gas flow rate at 8.0 L/min, nebulizer gas pressure at 1.5 bar, and dry gas temperature at 200 °C.

Results and Discussion

Electrical detection of interactions between angiotensin II and lysenin channels

Before lysenin addition, the absence of any conducting pathway was indicated by the absence of ionic currents through the planar BLM, which is an insulator. The step wise variation of the ionic current after lysenin addition at -60 mV bias potential was indicative of channel insertion (Figure 4a). The ratio I/V directly provided the individual conductance of a channel (~ 2 nS), which is larger than what was previously estimated from measurements performed in low ionic strength conditions. However, there is no inconsistency with our measurements owing to the large ionic conductivity presented by the 1 M KCl support electrolyte solution. The same individual channel conductance was estimated after insertion of two lysenin channels into the membrane biased by -80 mV (Figure 4), indicative of channel uniformity.

A steady and quiet baseline of the ionic current through two lysenin channels was observed at -80 mV and high temporal resolution before adding the analyte to be studied, indicate the absence of gating. The remarkable low noise of the trace (< 2.6 pA RMS at 10 kHz bandwidth) suggests an excellent suitability of lysenin channels for discriminating very small changes of the ionic currents, hence indicating an improved sensitivity. Addition of 1 μg ml^{-1} Ang II into the *trans* (headstage) reservoir at -80 mV bias potential elicited no changes of the ionic currents recorded in otherwise similar conditions (Figure 4c). This is a clear indication of the absence of interactions between channels and analyte molecules. However, analyte addition to the *cis* (ground) reservoir at the same concentration elicited numerous transient changes of the ionic current, suggesting strong interactions between the peptides and inserted channels [7, 21-23, 55-59]. These first observations point out that channel-analyte interactions are promoted only for particular orientation of the external electric field. Ang II bears a small positive charge near neutral pH and it is expected to interact with electric fields. The electric field inside the bulk electrolyte solution is very low owing to the high conductance but it is not negligible. Apparently, the peptides added to the *trans* reservoir are electrophoretically driven away from the membrane. The random thermal motion may bring the peptides close to the channels but the increasing fringe electric field may drive them away. The electric field increases considerably as the peptides move closer to the pore opening and the resulting electric force will drive the analytes away therefore preventing penetration into the channel. By switching the direction of the electric field, the peptides are electrophoretically driven towards the nanopore, captured by the fringe electric field, and forced to translocate through the channel by the large transmembrane electric field. A

closer inspection of the transient electronic signature (inset Figure 4d) shows transient changes in the ionic currents typical to molecule translocation through nanopores.

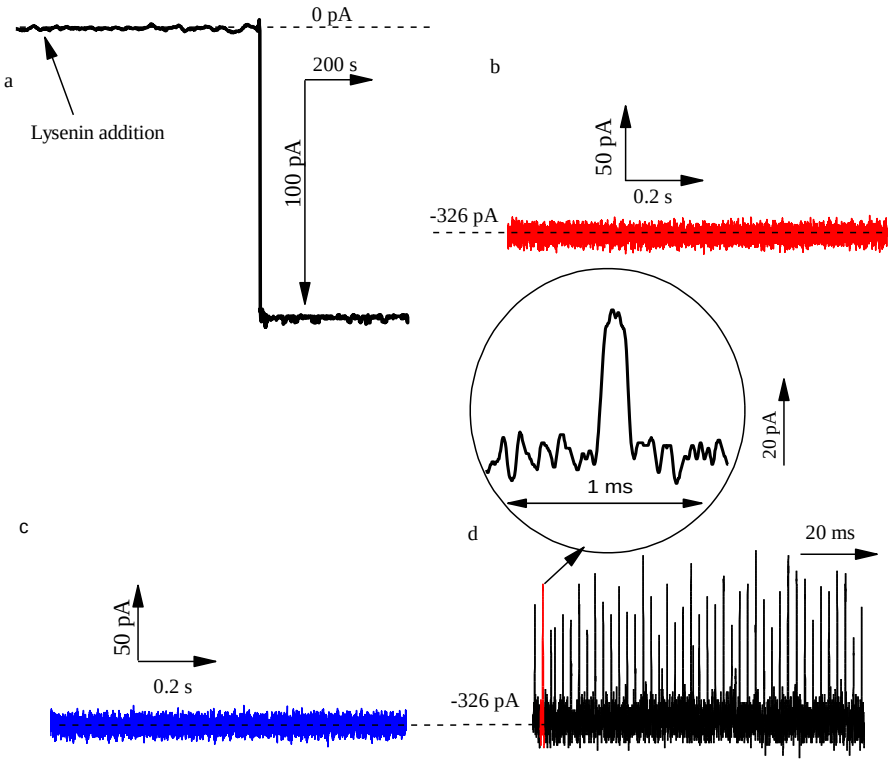

Figure 4. Interactions of Ang II with single lysenin channels produce transient changes in ionic currents. a) Insertion of a single channel into the lipid membranes containing the electrolyte solution (1 M KCl with 10 mM Tris and 1 mM EDTA, pH 6.9) results in an increase magnitude of current at -60 mV transmembrane potential (sampling time 1 s, 1 kHz low pass hardware filter, and 10 Hz low pass software filter). b-c) Absence of transient changes in the ionic current via single lysenin channels at -80 mV when Ang II b) was not added to the reservoirs and c) added only to the trans side. d) Addition of the peptide to the cis reservoir at -80 mV produced temporary blockages in the ionic current, indicating the interaction between the single lysenin channels and Ang II. (Adapted from Shrestha et al. (2017) [53])

Event analysis, classification, and interpretation

The transient changes in the ionic currents elicited by interactions between lysenin channels and Ang II clearly resemble electronic signatures observed in prior experiments comprising biological nanopores and peptides [7, 19, 23, 56-59]. To provide an in-depth analysis of the recorded events, we further analyzed transients by estimating the average current change during the transient blockage, $<I_B>$, and the dwell time, t_D, with the Transalyzer software package, specifically developed for analysis of translocation data [52]. The events recorded at -80 mV were analysed with Transalyzer software and the density map was plotted with Origin software (Figure 5a). We immediately observed that the events are clustered into two distinct classes, which we named E1 and E2. Such clustering is typical for macromolecule translocation through either synthetic or natural nanopores [7, 19, 56, 60], and may originate in unsuccessful translocation attempts when the molecules only collide with the channel opening [7, 56], different orientation of molecules entering the nanopore [4], folding, oligomerization [19], or analyte binding to the pore lumen [59].

What is obvious is that the two classes of events are quite distinct, which is not common for translocation experiments employing peptides as analytes. Given the large separation of the two classes, we succeeded to perform individual analyses on each class, which allowed a better interpretation of the origin of clustering. The $<I_B>$ distributions were narrow and symmetric (Figure 5b), with peaks centered at ~26 pA (E1 events) and ~10 pA (E2 events).

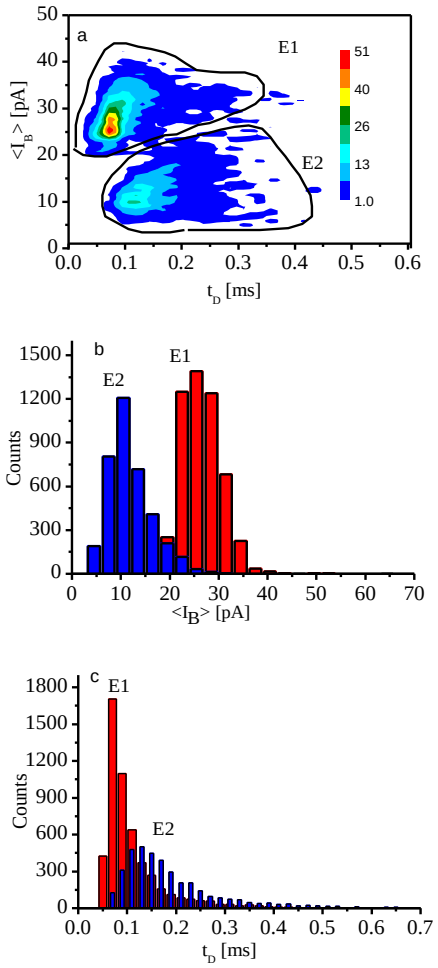

Figure 5. Analysis of transient blockages of the ionic current after addition of Ang II to the cis reservoir at -80 mV produces two types of events. a) The density plot indicates two clearly distinguishable events type E1 and E2. b) Distribution of <IB> histograms (bin width 3 pA) gives peak currents of E1 events at ~26 pA and E2 events at ~10 pA, respectively. c) Distribution of tD histograms (bin width 0.02 ms) presents peak of E1 events at ~70 µs and E2 events at ~120 µs, respectively. In order to clearly distinguish the overlapped distribution, a gap between the bins for the E2 events was included. (Adapted from Shrestha et al. (2017) [53])

Both values of the average current blockage are very small relative to the open current (less than ~25%), while other translocation experiments employing peptides or short polynucleotides interacting with synthetic or biological nanopores report larger ratios [6, 7, 11, 23, 56]. To explain this particular observation, we inspected the physical

properties of the channel and peptide. The lysenin channel is uniform and has a length of ~ 10 nm, which is comparable to the aerolysin channel and longer than α-HL. Structural data and electrical measurements indicate that the lysenin channel diameter is larger than either aerolysin or α-HL, thus suggesting larger inner volume of the conducting pathway. The analyte Ang II is a short peptide consisting of only eight amino acids. The contour length of the peptide is not known but we may assume it is shorter than the peptides containing more amino acids and tested for translocation in experiments comprising α-HL or aerolysin [7, 56]. The small contour length and hydrodynamic diameter of the peptide compared to the nanopore suggest that analyte passage may elicit relatively small changes in the ionic currents by displacing only a fraction of the total volume; such a feature has been previously reported for translocation of short peptides through the large channel of hetero-oligomeric channel from *Nocardia farcinica* [59].

Further analysis of the events recorded at -80 mV in terms of dwell time distribution (Figure 5c) showed skewed, non-symmetrical and overlapped histograms for the two event types. In addition, the E2 distribution spanned a broad range of dwell time values, while the E1 distribution was narrower, and such features were also observed in the density plot presented in Figure 5a. The major peaks at ~70 μs (E1 events) and ~120 μs (E2 events) were still well separated but the skewness clearly produce large discrepancies between peak and average values. In spite of such shortcomings, the time distributions are different than what is customarily presented for translocation of peptides and short polynucleotides through biological channels, i.e. exponential decays described by characteristic relaxation times as a measure of mean t_D [7, 11, 19, 21, 23, 56, 59]. In addition, these previous analyses “force” an exponential distribution of the dwell time,

which presents several notable drawbacks. An exponential distribution tacitly assumes that the maximum value is obtained for a dwell time close to zero. However, irrespective of the recording device, shorter events are always filtered and their shape significantly altered. Also, to eliminate the high frequency noise, a low-pass filter is always employed for data recording, which may critically affect short events by changing their shape and shift the time distribution. Nonetheless, our results cannot be accurately described as a combination of exponential decays. Given the electrical quietness of the lysenin channels, we successfully triggered the event recording such that the electrical noise was eliminated from the traces at 4 µs sampling time and 10 kHz hardware filter. The time distributions rather resemble gamma functions instead of exponential functions and the peak values are far from zero, which is what is expected from translocation experiments. This is consistent with the exponential description since the gamma function is mathematically reducible to an exponential, for which the mean value is the relaxation time. However, no current translocation model provides mechanistic insights to justify such a distribution.

Analysis of the transient events recorded at different voltages is a helpful tool for data interpretation in terms of identifying the origin of specific electronic signatures, i.e. putative translocations versus collisions [56, 61]. The E1 events recorded at voltages ranging from -40 mV to -100 mV showed a linear relationship of the mean $<I_B>$s for the entire voltage range (Figure 6a). This is indicative of putative translocation [7] since the currents are proportional to voltages for ohmic behaviors, i.e. the applied voltage does not affect the conductance. The analysis of the E2 events indicated a minor influence of the applied voltage on currents, which is characteristic to failed translocation attempts, i.e. molecules bumping into the pore and diffusing away [7]. Both E1 and E2 events were

characterized by a decrease of the mean t_D for increases in the transmembrane voltage (Figure 6b). However, the E2 events presented a greater influence of the applied voltage on the dwell time, while the E1 events underwent less pronounced changes. This observation seems inconsistent with studies showing that the applied voltage may strongly influence the t_D of putative translocations [59]. However, a recent report shows [6] that the translocation time of short and weakly charged molecules is less influenced by voltage, probably due to a greater contribution from diffusion. Nonetheless, diffusion alone is not expected to overcome the significant electrostatic barrier presented by the large electric field inside the channel and to allow diffusive-only translocation.

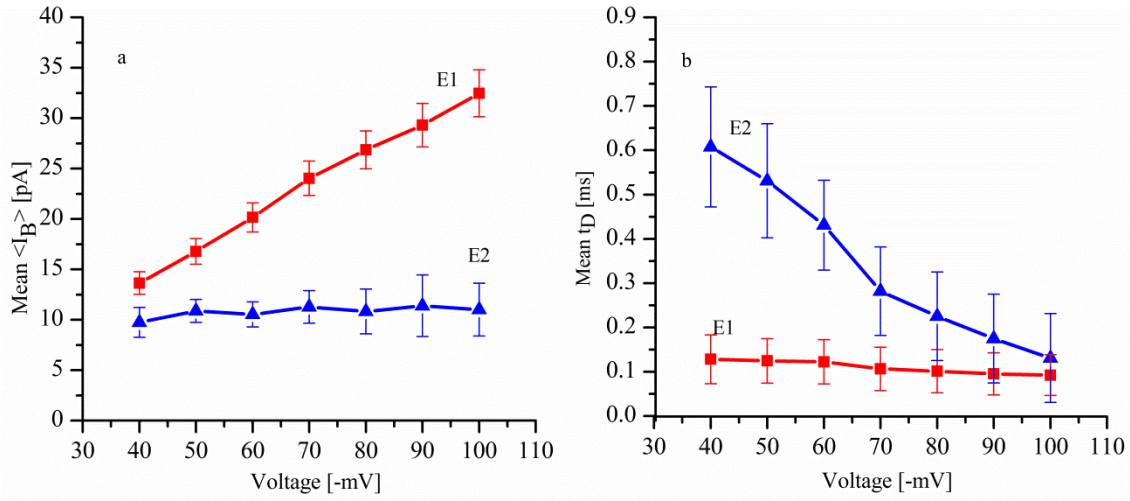

Figure 6. Mean current blockages and mean dwell time as a function of the applied voltage. a) The mean <IB> of events E1 (squares) increased linearly with the applied voltage, suggesting putative translocation. On the other hand, E2 events (triangles) had minimal effects in response to the applied voltage. b) The mean tD of both E1 (squares) and E2 (triangles) events decreased with the applied voltage. (mean ± S.D, n=3). (Adapted from Shrestha et al. (2017) [53])

Investigations focused on effects of applied voltage on translocation of either short nucleotides or peptides indicate a quasi-linear dependency of the frequency of interactions for voltage ranges similar to what we used for our experiments [6, 21]. Our

analysis performed on each class of events, i.e. E1 and E2, showed a similar linear dependency (Figure 7). The number of counts per time unit varied significantly between the three independent experiments, as indicated by the large deviations, but each one presented the same trend. Also, we observed that the frequency varied with time and it was greater at the end of each experiment, which we explained by considering the accumulation of the analyte in the vicinity of the channels owing to the electrophoretic force. Nonetheless, the slopes of the plots were relatively uniform and equal; indicating that for each voltage in the range of the ratio between translocations and collisions was close to unitary.

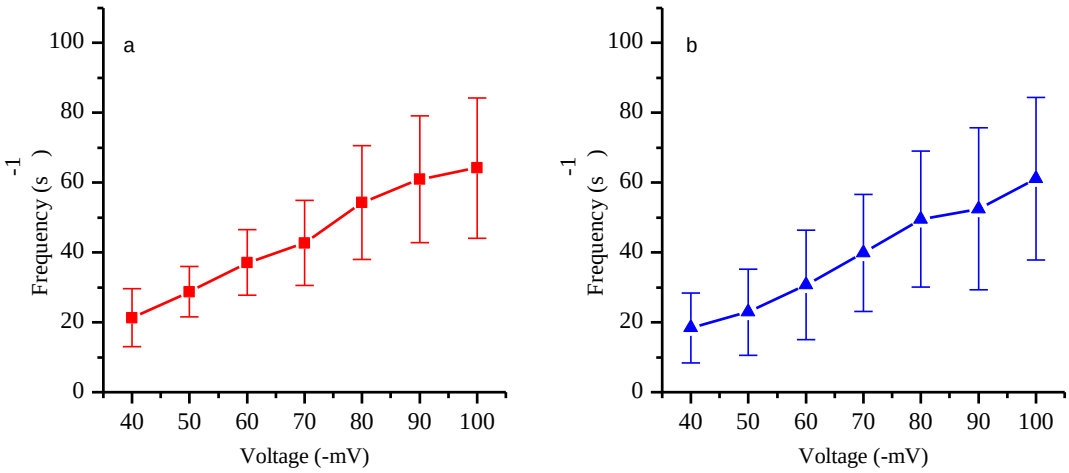

Figure 7. Voltage dependence of the frequency of E1 events (a) and E2 events (b) per single nanopore. The experimental points represent mean ± SD, n = 3. (Adapted from Shrestha et al. (2017) [53])

Liquid chromatography-mass spectroscopy analysis of angiotensin II translocation through large populations of lysenin channels

Since the first use of α-HL for DNA translocation, PCR amplification has proven to be very effective for detection and identification of translocated nucleic acid molecules [1]. However, such techniques are not available for peptide amplification, and their

detection and identification is seriously challenged by the very low amounts resulting from translocation experiments [11, 19, 62], which are difficult to analyze by any current methodology. To circumvent this roadblock, qRT-PCR has been used to identify translocated chimeric DNA-peptide molecules [55]; however, the analyte was structurally different, which raises the question if the DNA was actually the carrier of the peptide. Similarly, addition of fluorescent tags may structurally change the molecules and strongly affects their interactions with the channels, thus introducing undesired variables in the experimental setup. A great advancement in this line was reported for detection, identification, and quantitation of proteins translocated through synthetic nanopores [62]. To enable such achievement, the analyte was translocated for extended time through a silicon nitride nanopore at large bias potentials and the assessment was performed by using a very sensitive chemiluminescence-based approach [62]. However, the bilayer lipid membranes are rather fragile structures, their lifetime is limited, and the application of large transmembrane potentials leads to premature rupture owing to the large transmembrane electric field. However, the synthetic nanopore experiments indicate that translocated protein molecules may be detected and identified with high sensitivity techniques if sufficient molecules are accumulated. To increase the amount of translocated peptide, we adjusted both the number of lysenin channels inserted into the membranes and the duration of the experiments [45, 51]. After Ang II translocation through large populations of lysenin channels at -100 mV bias potential, samples from the *trans* reservoirs have been subjected to LC-MS analysis along with a standard sample containing 100 ng peptide. The presence of Ang II in the *trans* reservoir was clearly indicated by both LC and MS (Figure 8 c,d). However, supplementary evidence was

needed to demonstrate that the analyte passed through lysenin channels. At high concentration, Ang II is capable of interacting with pristine artificial lipid membranes [63, 64]. This interaction is manifested as either pore formation [63], and hence an increased permeability, or a sustained adsorption at the membrane surface [64], which may promote further transmembrane transport.

To eliminate any concern with regards to non-specific Ang II transport through artificial membranes, we performed extended experiments of Ang II translocation through large populations of lysenin channels biased by positive potentials (+100 mV). Although lysenin channels may gate at positive voltages, high salt concentration and congested conditions almost completely eliminate this feature, and most of the channels will remain in the high conducting state in such experimental conditions [45, 51]. The requirement of proper orientation of the external electric field for enabling translocation was inferred from the absence of LC signal in the sample collected from the *trans* reservoir after 36 hours of exposure to positive voltages (Figure 8e). Still, the absence of a signal may be simply linked to the opposite electrophoretic force created by the reverse electric field, which will prevent translocation through either open channels or membrane permeabilized by Ang II. To further support the hypothesis of Ang II translocation only through open channels, the next experiment employed the use of large populations of lysenin channels in which the membrane was biased by -100 mV (to promote translocation) but the channels were irreversibly blocked by chitosan addition as described in the methods section and elsewhere [54]. The LC analysis of samples collected from the *trans* reservoir showed the absence of Ang II (Figure 8f); while it is still possible that spontaneous transmembrane translocation of Ang II at levels below the

LC-MS detection limit occurred, clearly open lysenin channels inserted into the membrane are needed to mediate peptide translocation at detectable levels.

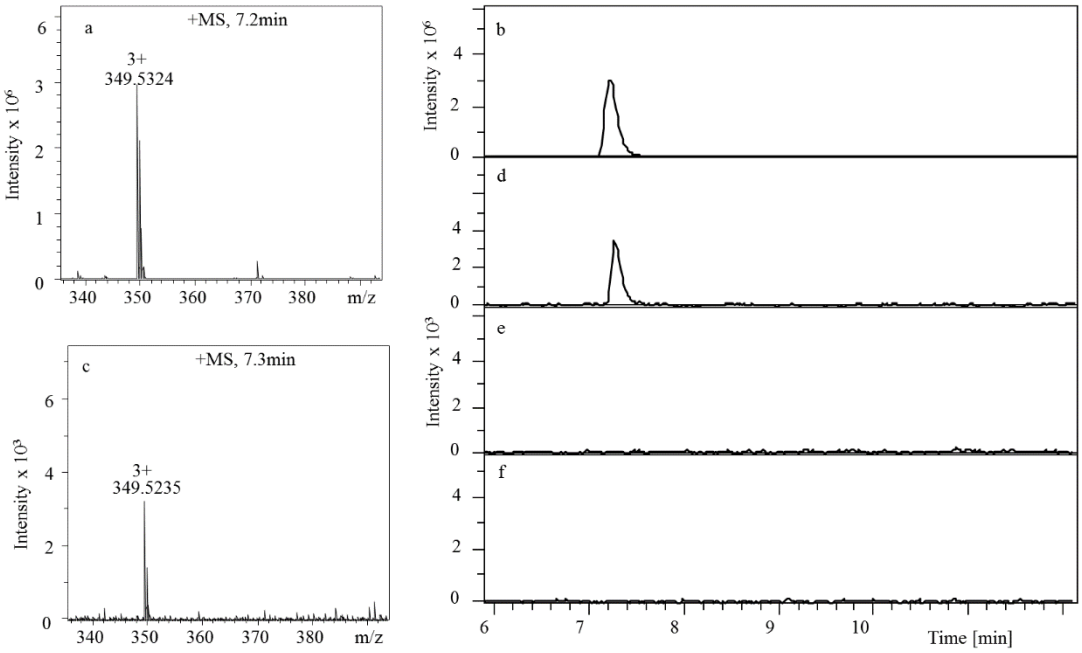

Figure 8. Verification of the translocation of Ang II using LC-MS after running the experiments in the presence of large population of lysenin channels for 36 hours at -100 mV. a) The MS of standard Ang II (100 ng) with m/z of 349.5 (z = 3+), b) LC chromatogram of standard 100 ng Ang II, c) The translocated samples collected from trans reservoir after application of -100 mV for 36 hours indicated the presence of Ang II by (c) MS and (d) LC. In the similar condition, LC did not detect Ang II on the trans solution when (e) applying +100 mv voltage, and (f) blocking the channels with chitosan. [53]

By integrating the LC peak areas for Ang II amounts in the range 1 ng-100 ng (Figure 9a), a standard calibration curve was constructed (Figure 9b) and used to estimate the total amount of peptide translocated through the large population of lysenin channels (~ 0.8 ng). By equating this amount to the total number of channels and duration, we computed a translocation frequency of ~1,100 events/s, which is practically twice as much as the average value estimated from single channel experiments at the same voltage

(see Figure 7). This discrepancy may be explained by accounting for the large deviations in the frequency data, which may originate in their time-dependency resulting from local accumulation of the analyte in the vicinity of the channel. However, the hypothesis that both type of events represent translocations is not consistent with the observed effects of voltage on the current blockages and dwell times characteristic to the two distinct event types.

a.

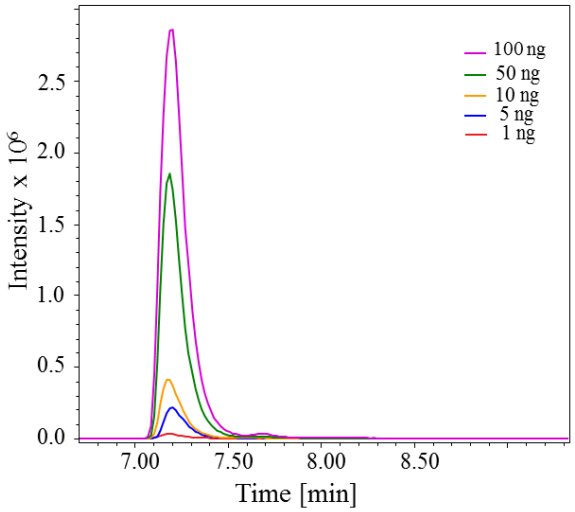

b.

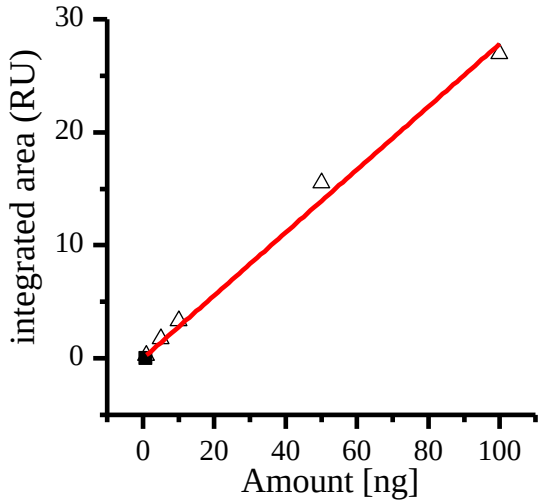

Figure 9. The LC chromatograms of standard Ang II. a) The LC chromatograms of known Ang II obtained from the different amount of Ang II from 1-100 ng. b) The standard curve (triangles) obtained from the integrated area under the curve as shown in (a) to determine the unknown concentration of Ang II (full square).

Conclusions

Lysenin channels inserted into artificial lipid membranes present a great potential for single molecule sensing and characterization. By employing single channels and Ang II we demonstrated that lysenin allows the translocation of un-modified peptides, and therefore may be used for stochastic sensing using the resistive pulse technique. The large

diameter of the channel enables analysis of molecules larger than what may be used with other nanopores of biological origin. The absence of vestibular structures and constrictions yields events that are easily classified as putative translocations or collisions. No other biological nanopores provide such a clear distinction between the two event types when peptide molecules are used as analytes. The excellent stability of lysenin channels reconstituted in bilayer lipid membranes demonstrated that translocation requires the molecules to be electrophoretically driven through the open channels. This is the first proof of translocation of un-altered peptide molecules through a biological nanopore. LC-MS allowed not only peptide identification but quantitation, which satisfactorily matched the experimental data originating in single channel experiments. Lysenin also presents biophysical properties that are uncommon among PFTs, such as reversible gating or irreversible blockage. These unique regulatory mechanisms, in conjunction with bio-engineering approaches may be used to further expand the sensing capabilities beyond translocation and design a new class of smart biosensors and bioactuators with applicability in early diagnosis, drug delivery, and self-control of micro bioreactors.

Acknowledgements

The experimental data from Figures 2, 3, 4, 5, 6, 7, and 8 have been published by the author of this dissertation under the terms of the Creative Commons Attribution (https://creativecommons.org/licenses/by/4.0) [53]. The original data did not suffer any alteration but data may be presented differently.

References

1. Kasianowicz, J.J., et al., *Characterization of individual polynucleotide molecules using a membrane channel.* Proceedings of the National Academy of Sciences of the United States of America, 1996. **93**(24): p. 13770-13773.

2. Wang, H.Y., et al., *Analysis of a single α-synuclein fibrillation by the interaction with a protein nanopore.* Analytical Chemistry, 2013. **85**(17): p. 8254-8261.

3. Wang, Y., et al., *Nanopore-based detection of circulating microRNAs in lung cancer patients.* Nature Nanotechnology, 2011. **6**(10): p. 668-674.

4. Butler, T.Z., et al., *Single-molecule DNA detection with an engineered MspA protein nanopore.* Proceedings of the National Academy of Sciences, 2008. **105**(52): p. 20647-20652.

5. Haque, F., et al., *Solid-state and biological nanopore for real-time sensing of single chemical and sequencing of DNA.* Nano Today, 2013. **8**(1): p. 56-74.

6. Cao, C., et al., *Discrimination of oligonucleotides of different lengths with a wild-type aerolysin nanopore.* Nature Nanotechnology, 2016. **11**(8): p. 713-718.

7. Stefureac, R., et al., *Transport of a-helical peptides through a-hemolysin and aerolysin pores.* Biochemistry, 2006. **45**(30): p. 9172-9179.

8. Wendell, D., et al., *Translocation of double stranded DNA through membrane adapted phi29 motor protein nanopore.* Nature Nanotechnology, 2009. **4**(11): p. 765-772.

9. Wang, S., et al., *Engineered nanopore of Phi29 DNA-packaging motor for real-time detection of single colon cancer specific antibody in serum.* ACS Nano, 2013. **7**(11): p. 9814-9822.

10. Butler, T.Z., J.H. Gundlach, and M. Troll, *Ionic current blockades from DNA and RNA molecules in the α-hemolysin nanopore.* Biophysical Journal, 2007. **93**(9): p. 3229-3240.

11. Cao, C., et al., *Driven translocation of polynucleotides through an aerolysin nanopore.* Analytical Chemistry, 2016. **88**(10): p. 5046-5049.

12. Ashton, P.M., et al., *MinION nanopore sequencing identifies the position and structure of a bacterial antibiotic resistance island.* Nature Biotechnology, 2014. **33**(3): p. 296-300.

13. Kilianski, A., et al., *Bacterial and viral identification and differentiation by amplicon sequencing on the MinION nanopore sequencer.* Gigascience, 2015. **4:** p. 12. doi: 10.1186/s13742-015-0051-z

14. Lu, H., F. Giordano, and Z. Ning, *Oxford Nanopore MinION Sequencing and Genome Assembly.* Genomics Proteomics Bioinformatics, 2016. **14**(5): p. 265-279.

15. Mikheyev, A.S. and M.M. Tin, *A first look at the Oxford Nanopore MinION sequencer.* Molecular Ecology Resources, 2014. **14**(6): p. 1097-1102.

16. Quick, J., A.R. Quinlan, and N.J. Loman, *A reference bacterial genome dataset generated on the MinION portable single-molecule nanopore sequencer.* GigaScience, 2014. **3**(1): p. 22. doi: 10.1186/2047-217X-3-22

17. Loman, N.J. and M. Watson, *Successful test launch for nanopore sequencing.* Nature methods, 2015. **12**(4): p. 303-304.

18. Bayley, H., *Nanopore sequencing: from imagination to reality.* Clinical chemistry, 2015. **61**(1): p. 25-31.

19. Ji, Z., et al., *Fingerprinting of peptides with a large channel of bacteriophage Phi29 DNA packaging motor.* Small, 2016. **12**(33): p. 4572–4578.

20. Meng, H., et al., *Nanopore analysis of tethered peptides.* Journal of Peptide Science, 2010. **16**(12): p. 701-708.

21. Movileanu, L., et al., *Interactions of peptides with a protein pore.* Biophysical Journal, 2005. **89**(2): p. 1030-1045.

22. Sutherland, T.C., et al., *Structure of peptides investigated by nanopore analysis.* Nano Letters, 2004. **4**(7): p. 1273-1277.

23. Zhao, Q., et al., *Study of peptide transport through engineered protein channels.* The Journal of Physical Chemistry B, 2009. **113**(11): p. 3572-3578.

24. Blennow, K., et al., *Amyloid biomarkers in Alzheimer's disease.* Trends in Pharmacological Sciences, 2015. **36**(5): p. 297-309.

25. Ni, J., et al., *Role of the EpCAM (CD326) in prostate cancer metastasis and progression.* Cancer and Metastasis Reviews, 2012. **31**(3): p. 779-791.

26. Niedzwiecki, D.J., et al., *Sampling a biomarker of the human immunodeficiency virus across a synthetic nanopore.* ACS Nano, 2013. **7**(4): p. 3341-3350.

27. Mor, G., et al., *Serum protein markers for early detection of ovarian cancer.* Proceedings of the National Academy of Sciences, 2005. **102**(21): p. 7677-7682.

28. Li, Y., et al., *Association between serum C-peptide as a risk factor for cardiovascular disease and high-density lipoprotein cholesterollLevels in nondiabetic individuals.* PLoS ONE, 2015. **10**(1): p. e112281. doi: 10.1371/journal.pone.0112281

29. Min, J.-Y. and K.-B. Min, *Serum C-peptide levels and risk of death among adults without diabetes mellitus.* Canadian Medical Association Journal, 2013. **185**(9): p. E402-E408.

30. Nivala, J., D.B. Marks, and M. Akeson, *Unfoldase-mediated protein translocation through an [alpha]-hemolysin nanopore.* Nature Biotechnology, 2013. **31**(3): p. 247-250.

31. Payet, L., et al., *Thermal unfolding of proteins probed at the single molecule level using nanopores.* Analytical Chemistry, 2012. **84**(9): p. 4071-4076.

32. Biesemans, A., M. Soskine, and G. Maglia, *A Protein rotaxane controls the translocation of proteins across a ClyA nanopore.* Nano Letters, 2015. **15**(9): p. 6076-6081.

33. Soskine, M., et al., *An engineered ClyA nanopore detects folded target proteins by selective external association and pore entry.* Nano Letters, 2012. **12**(9): p. 4895-4900.

34. Haque, F., et al., *Single pore translocation of folded, double-stranded, and tetra-stranded DNA through channel of bacteriophage phi29 DNA packaging motor.* Biomaterials, 2015. **53**: p. 744-752. doi: 10.1016/j.biomaterials.2015.02.104

35. Beamish, E., et al., *Fine-tuning the size and minimizing the noise of solid-state nanopores.* Journal of Visualized Experiments, 2013(80): p. e51081. doi: 10.3791/51081

36. Briggs, K., H. Kwok, and V. Tabard-Cossa, *Automated fabrication of 2-nm solid-state nanopores for nucleic acid analysis.* Small, 2014. **10**(10): p. 2077-2086.

37. Tao, D., et al., *Development of solid-state nanopore fabrication technologies.* Science Bulletin, 2015. **60**(3): p. 304-319.

38. Bayley, H. and P.S. Cremer, *Stochastic sensors inspired by biology.* Nature, 2001. **413**(6852): p. 226-230.

39. Bell, N.A.W. and U.F. Keyser, *Digitally encoded DNA nanostructures for multiplexed, single-molecule protein sensing with nanopores.* Nature Nanotechnology, 2016. **11**(7): p. 645-651.

40. Rosen, C.B., D. Rodriguez-Larrea, and H. Bayley, *Single-molecule site-specific detection of protein phosphorylation with a nanopore.* Nature Biotechnology, 2014. **32**(2): p. 179-181.

41. Bokori-Brown, M., et al., *Cryo-EM structure of lysenin pore elucidates membrane insertion by an aerolysin family protein.* Nature Communications, 2016. **7**. doi: 10.1038/ncomms11293

42. Podobnik, M., et al., *Crystal structure of an invertebrate cytolysin pore reveals unique properties and mechanism of assembly.* Nature Communications, 2016. **7**: p. 11598. doi: 10.1038/ncomms11598

43. De Colibus, L., et al., *Structures of lysenin reveal a shared evolutionary origin for pore-forming proteins and its mode of sphingomyelin recognition.* Structure, 2012. **20**(9): p. 1498-1507.

44. Fologea, D., et al., *Multivalent ions control the transport through lysenin channels.* Biophysical Chemistry, 2010. **152**(1-3): p. 40-45.

45. Fologea, D., et al., *Bi-stability, hysteresis, and memory of voltage-gated lysenin channels.* Biochimica et Biophysica Acta, Biomembranes, 2011. **1808**(12): p. 2933-2939.

46. Fologea, D., et al., *Potential analytical applications of lysenin channels for detection of multivalent ions.* Analytical and Bioanalytical Chemistry, 2011. **401**(6): p. 1871-1879.

47. Krueger, E., et al., *A model for the hysteresis observed in gatuing of lysenin channels.* Biophysical Chemistry, 2013. **184**: p. 126-130.

48. Fologea, D., et al., *Controlled gating of lysenin pores.* Biophysical Chemistry, 2010. **146**(1): p. 25-29.

49. Ide, T., et al., *Lysenin forms a voltage-dependent channel in artificial lipid bilayer membranes.* Biochemical and Biophysical Research Communications, 2006. **346**(1): p. 288-292.

50. Bryant, S., et al., *Purinergic control of lysenin's transport and voltage-gating properties.* Purinergic Signalling, 2016. **12**(3): p. 549-559.

51. Krueger, E., et al., *Intramembrane congestion effects on lysenin channel voltage-induced gating.* European Biophysics Journal, 2016. **45**(2): p. 187-194.

52. Plesa, C. and C. Dekker, *Data analysis methods for solid-state nanopores.* Nanotechnology, 2015. **26**(8): p. 084003.

53. Shrestha, N., et al., *Stochastic sensing of Angiotensin II with lysenin channels.* Scientific Reports, 2017. **7**. doi: 10.1038/s41598-017-02438-0

54. Fologea, D., et al., *Cationic polymers inhibit the conductance of lysenin channels.* The Scientific World Journal, **2013**. doi: 10.1155/2013/316758

55. Pastoriza-Gallego, M., et al., *Evidence of unfolded protein translocation through a protein nanopore.* ACS Nano, 2014. **8**(11): p. 11350-11360.

56. Stefureac, R., et al., *Nanopore Analysis of a small 86-residue protein.* Small, 2008. **4**(1): p. 59-63.

57. Lamichhane, U., et al., *Peptide translocation through the mesoscopic channel: binding kinetics at the single molecule level.* European Biophysics Journal, 2013. **42**(5): p. 363-369.

58. Mereuta, L., et al., *Slowing down single-molecule trafficking through a protein nanopore reveals intermediates for peptide translocation.* Scientific Reports, 2014. **4**. doi: 10.1038/srep03885

59. Singh, P.R., et al., *Pulling peptides across nanochannels: Resolving Peptide Binding and Translocation through the Hetero-oligomeric Channel from Nocardia farcinica.* ACS Nano, 2012. **6**(12): p. 10699-10707.

60. McMullen, A., et al., *Stiff filamentous virus translocations through solid-state nanopores.* Nature Communications, 2013. **5**. doi: 10.1038/ncomms5171

61. Madampage, C.A., O. Andrievskaia, and J.S. Lee, *Nanopore detection of antibody prion interactions.* Analytical Biochemistry, 2010. **396**(1): p. 36-41.

62. Fologea, D., et al., *Electrical characterization of protein molecules by a solid-state nanopore.* Applied Physics Letters, 2007. **91**(5): p. 053901-1-053901-3.

63. Hianik, T. and G. Laputkova, *Angiotensin II-induced formation of ionic channels in bilayer lipid membranes.* General Physiology and Biophysics, 1991. **10**(1): p. 19-30.

64. Jalili, P.R. and C. Dass, *Determination of the structure of lipid vesicle-bound angiotensin II and angiotensin I.* Analytical Biochemistry, 2008. **374**(2): p. 346-357.

CHAPTER THREE: LYSENIN CHANNELS AS NANO-SWITCHES FOR CONTROLLED MEMBRANE PERMEABILITY

Abstract

The functionality of cells may be modulated by numerous classes of exogenous molecules such as nucleic acids, homing peptides, and small activators and inhibitors. In many instances, these molecules must cross the plasma membrane to exert their biological effect, and this is often realized by specific or non-specific transport mechanisms employed by cells. However, the plasma membrane presents a high selectivity, and therefore constitutes a barrier that prevents the access of extra-cellular molecules to the cytosol. Overcoming the selective nature of the membrane enables manipulating fundamental cellular functionalities and presents opportunities to target, identify and investigate distinct molecules or cellular processes. To achieve this goal, controlled access to the cytosol may be achieved by microinjection, electroporation, optoporation, lipovesicles, and cell-penetration peptides. Each of these techniques have limitations such as single-cell applicability, invasiveness, low efficiency, expensiveness, tedious procedures, or the necessity of using sophisticated dedicated instruments. In addition, biomedical and scientific applications may require transmembrane transport into small artificial lipid vesicles, which are not easy to permeabilize by using the above methods. To overcome many of these barriers, we propose to use lysenin for temporary permeabilization of artificial and natural lipid membranes. Lysenin is a pore-forming

toxin extracted from the earthworm *Eisenia fetida*, which inserts large conducting channels into lipid bilayer membranes containing sphingomyelin. The large opening of the channel is expected to accommodate the passage of relatively large molecules significant for scientific, bio-technological and biomedical purposes. The choice of lysenin is also motivated by the presence of unique regulatory mechanisms that employs external physical and chemical stimuli, thereby enabling exquisite control over membrane permeability.

The work hereby aims at demonstrating that lysenin channels may be used as nano-switches for controlling the permeability of artificial and natural membrane systems. Experiments employing electrophysiology explorations of ionic transport demonstrate that ATP may reversibly control the macroscopic conductance of lysenin channels reconstituted into planar lipid membranes. Investigations performed on unilamellar liposomes show that non-permeant dyes may be loaded in the inner water-filled cavity through transmembrane diffusion mediated by lysenin channels. Further explorations demonstrate that the permeabilized membrane can be resealed by multivalent cations that force the channels to close. In addition, cation removal by precipitation re-opens the channels and allow the incorporated dye to leak out. Next, we investigated the lysenin-mediated transport of cell impermeant fluorescent molecules into two distinct cell lines, Jurkat and ATDC5, respectively. Careful selection of dead/live fluorescent dye allowed us to assess both permeabilization efficiency and survival rate. In addition, we successfully demonstrated that bio-inert chitosan polymer molecules can be used to effectively turn off the lysenin-induced permeability by irreversible channel blockage.

Introduction

The highly regulated transport of ions and molecules across cell membranes is paramount for fundamental cellular processes such as nutrient transport, energy production, transmission of information, or communication [1-7]. To overcome the natural barrier function presented by the lipid membrane, cells developed specialized transporters capable of selective transport in response to chemical or physical stimuli. However, assessing, controlling, or introducing novel cellular functionalities for the purpose of cellular or molecular manipulation requires non-invasive introduction of biologically relevant molecules into living cells, which is greatly challenged by the same selective nature of the plasma membrane. To overcome the membrane barrier and gain access to the cytosol, a number of techniques have been developed and employed over the years. Microinjection is one of the most commonly used techniques but is tedious, invasive, requires experienced personnel, and is limited to single cells [8]. Electroporation, or electrical pore formation in cell membranes under exposure to an external electric field, is very popular for cytosol entrapment of exogenous macromolecules, including foreign genes [9]. However, the strong external electric field needed for efficient electroporation often leads to low efficiency by significantly diminishing cell viability [10]. Optoporation, another non-contact method of single-cell permeabilization, requires sophisticated instruments [11] and may suffer from undesired interactions between the strong laser light and strong absorbers present in the exposed cell. Lipovesicles, lipophilic carriers and cell-penetrating peptides are included with intracellular delivery methods which are efficient in the delivery of DNA but often have limitations presented by cargo trapping in endosomal and lysosomal vesicles [12-15]. In

spite of wide applicability of the above methods in science, technology, and medicine, scientists are actively pursuing other more effective approaches for delivery of foreign molecules into living cells while maintaining cell viability. This is justified by the recognition that methods for controlled transport across natural and artificial membranes hold significant potential to revolutionize the field of science, biomedicine, and nanotechnology [16-20]. Externally controlled transport of exogeneous molecules through lipid membranes would not only provide novel insights into the functionality of cells and enable modulation of essential cellular functions but would provide opportunities for localized and controlled drug delivery, or novel design of nano-vesicles and smart bioreactors for biomolecule production.

Pore-forming proteins (PFPs) are among the most sought after gate-keepers for initiating and controlling the transmembrane transport in artificial and natural membrane systems. These pores provide nano-sized conducting pathways for the transport of molecules across membranes. Streptolysin-O, a cytolytic exotoxin from streptococci, forms large pores (up to ~30 nm diameter) in membranes containing cholesterol [21]. Owing to its large size, this toxin is able to deliver exogenous non-permeant molecules to the cytosol, including oligonucleotides, proteins, and dyes [21-24]. An engineered α-hemolysin (α-HL) from *Staphylococcus aureus* was designed as a metal-actuated switch for closing and reopening using Zn^{2+} ions and chelating agents [20]. The incorporation of α-HL in artificial vesicles paved the way to investigating transient and weak interactions of biological molecules in confined nano-vesicles [25].The large conductance pore of the bacterial mechanosensitive channel MscL (>2.5 nm diameter) was engineered in such a way to make it responsive to light and pH, and to deliver molecules into mammalian cells

[26-29]. In addition, MscL was embedded into an artificial system for releasing the entrapped solvent content [30]. The *E.coli* porins OmpF and Tsx have been included in the "membrane" walls of bioreactors encapsulating prodrug-activating enzymes [31]. The small prodrugs transported inside through the porins become activated and diffuse out as active drugs. Listeriolysin-O from *Listeria monocytogenes* and C2 toxin from *Clostridium botulinum* have shown promising results in mediating the transport of biologically active molecules across the membrane barrier [32-37].

All the above studies demonstrate PFP's applicability in facilitating the transport of otherwise non-permeant molecules across membranes. However, there are limitations for their use as controlled transporters, such as: cumbersome isolation and purification, difficult reconstitution in artificial or natural membrane systems, absence of high resolution structural data, premature leakage at rest, and lack of intrinsic regulatory mechanisms. To overcome these limitations and to develop nano-switches for controlled permeability, we propose using lysenin channels reconstituted into artificial and natural lipid membranes.

Why lysenin? Lysenin is a 297 amino acid PFP extracted from the coelomic fluid of the earthworm *Eisenia fetida* [38-40]. Although lysenin has no determined physiological role in the host organism, its strong cytolytic and hemolytic activity [39, 41, 42] is related to the ability to self-insert a large nonameric pore of ~ 3 nm diameter in artificial and natural membranes containing sphingomyelin [43-50]. This large lysenin pore provides an excellent opportunity for transporting relatively large molecules across the membrane in which it is inserted. The lysenin channel is larger than α-HL (which is ~1.5 nm diameter) [51], hence may ensure a higher transport rate and reduced steric

hindrance. In addition, lysenin channels possess intrinsic regulatory mechanisms that set it apart from other pore forming toxins and open novel avenues for the development of stimuli actuated nano-switches for controlled transport. Lysenin channels are regulated by transmembrane voltages in the physiological range [41, 52, 53]. The voltage-induced gating manifests as fast conformational transitions of the channel from conducting (open) to non-conducting (closed) state at transmembrane potentials larger than ~ 20 mV [41, 52, 53], potentially enabling the use of the channels as voltage-responsive nano-switches. Another salient regulatory feature of lysenin channels is the reversible regulation by multivalent ions [54, 55]. Trivalent metal cations including La^{3+}, Eu^{3+}, Ce^{3+}, Tb^{3+}, and Al^{3+} are very effective inhibitors and reduce the macroscopic conductance of lysenin channels to negligible values at concentrations of ~100 μM [54, 55]. The conductance blockage mechanism is based on ligand-gating and it is reversible since the initial conductance of each channel can be reinstated after ligand removal by addition of chelating or precipitating agents [54, 55]. This feature adds distinct opportunities for external control of the conducting state by using cations (i.e., multivalent metals) or anions (i.e., adenosine triphosphate-ATP) trapped in photolabile cages [56]. Another important characteristic of lysenin channels is their irreversible blockage by the positively charged polymers chitosan and polyethyleneimine [57], which may be used to reseal the membranes by blocking the lysenin channels and shutting down the transport.

In this study, we hypothesize that lysenin channels can be used to gain controlled permeability over artificial and natural lipid membranes. Planar bilayer lipid membrane (BLM) experiments were employed to study the reversible modulation of lysenin channel

conductance by ATP, along with irreversible blockage by chitosan in complex electrolytes. Studies performed on spherical lipid membranes (liposomes) demonstrated that the in and out traffic of non-permeant fluorescent molecules can be reversibly controlled by Al^{3+} cations and precipitating agents. Human acute T-cell leukemia Jurkat (suspension) and mouse chondrogenic ATDC5 (adherent) cells were used as models for investigating lysenin channels as transmembrane nanovalves for transport of non-permeant molecules. These studies included controlled permeability assays and viability assessments.

Materials and Methods

Preparation of planar bilayer lipid membranes

BLMs have been prepared in a custom-made chamber comprised of two ~1 ml reservoirs made of polytetrafluoroethylene (PTFE) and separated by a thin vertical PTFE film (~120 µM thickness, McMaster) in which a small hole (~70 µm diameter) was produced by an electric spark. The film was sandwiched between the two reservoirs with a thin layer of silicone grease to achieve a water-proof sealing. The bilayer was produced by the Montal-Mueller method [58], i.e. painting the hole with a small amount (< 1 µl) of a stock lipid mixture containing 10 mg asolectine (Aso, Sigma-Aldrich), 4 mg cholesterol (Chol, Sigma-Aldrich) and 4 mg sphingomyelin (SM, Avanti Polar Lipids) dissolved in 200 µl of n-decane (Alfa Aesar). The electrolyte solutions were 1X Hank's Balanced Salt Solution (1X HBSS, Thermo Fisher), or 135 mM KCl containing 20 mM HEPES, pH 7.2. Electrical connections to the headstage of the recording device (Axopatch 200B electrophysiology amplifier, Molecular Devices) have been provided by Ag/AgCl electrodes embedded in the solutions (Figure 1).

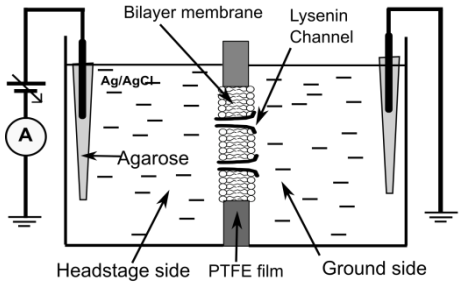

Figure 1. Simplified diagram (not to scale) of the experimental setup for studies employing bilayer lipid membranes. A planar lipid membrane created in a hole produced in a thin PTFE film serves as support for the insertion of lysenin channels. Two Ag/AgCl electrodes inserted into the electrolyte solutions bathing the membrane ensure electrical connections to the recording device. Optionally, the electrodes may be connected to the solutions via salt bridges. All BLM experiments were run in voltage-clamp mode.

The analog signal provided by the amplifier was fed into a DigiData 1440A digitizer (Molecular Devices) connected to a PC for real-time visualization and recording with the Clampex 10 software package (Molecular Devices). The formation of the membrane was monitored by indirectly estimating the membrane capacitance from the capacitive current measured in response to a triangle-shaped voltage stimulus and the integrity of the membrane was estimated from the leakage current measured in response to a DC voltage stimulus (100 mV). A "good" membrane was characterized by a capacitance of ~ 65 pF and a leakage current no greater than 0.1 pA, which corresponds to a seal resistance of at least 1000 GΩ. After a stable membrane was achieved, channel insertion was performed by adding lysenin to the ground reservoir under continuous stirring with a low noise Bilayer Magnetic Stirrer (Warner Instruments) at room temperature. The channel insertion process was monitored from the changes in the ionic current through the membrane biased by -60 mV [52, 53]. The completion of insertion was indicated by a steady value of the macroscopic ionic current; when this was

achieved, the un-inserted lysenin was removed from the bulk by buffer exchange with a lysenin-free electrolyte solution. ATP (Sigma-Aldrich) was prepared as 1 M stock solution by dissolving the powder in pure water. A stock chitosan solution was prepared by dissolving the chitosan (average M_w 200,000, Across Organics) in 0.1 M acetic acid at a final concentration of 1% (w/v). Propidium iodide (PI) and ethidium homodimer-1 (EtHD, Thermo Fisher) were prepared by solvation in 135 mM KCl at a final concentration of 1 mg/ml, and 2 mg/ml, respectively.

Preparation of liposomes

Liposomes were prepared by the extrusion method [59]. Chloroform solutions of 8 mg Aso, 2.5 mg SM, and 2.5 mg Chol were vacuum-dried overnight in a glass vial and the resulting lipid cake was slowly hydrated at 65^{o}C for five hours in 1 ml solution containing 135 mM KCl and 20 mM HEPES (pH 7.2). After each hour, the mixture was subjected to a freeze-thaw cycle by placing it in the freezer for twenty minutes, and immediately followed by immersion of the vial in hot water. Large aggregates visually observed in the solution after hydration were fragmented by short sonication (<10 seconds) in a benchtop sonicator. After the completion of hydration, the lipid solution containing multilamellar liposomes was extruded 40 times through stacked polycarbonate filters (1 µm pore diameter, Whatman) mounted in a Mini-Extruder (Avanti Polar Lipids) placed on a hotplate and kept at constant temperature (65^{o}C) for the entire duration of extrusion. After extrusion, the liposome solution was collected from the syringe, cooled down at room temperature and stored in refrigerator for further experiments. Image analysis was performed with a Nikon TS100 microscope equipped with an Infinity camera (Lumenera) and Nikon filter sets suitable for calcein. A stock solution of calcein

(50 µM) was prepared by dissolving it in 135 mM KCl, 20mM HEPES, pH 7.2. Calcein fluorescence quenching by multivalent ions (Al^{3+}, prepared as 10 mM solution in water from a 2 M $AlCl_3$ stock solution) was analyzed by using a Fluoromax 4P fluorometer (Horiba) set in emission mode (λ_{ex} = 485 nm, λ_{em} = 490nm - 550nm). The fluorescence spectrum of 50 µM calcein solution was recorded before and after successive addition of $AlCl_3$ solution to the sample in the cuvette under continuous stirring. The quenching curve was plotted as relative fluorescence intensity at 520 nm versus [Al^{3+}]. Al^{3+} removal was performed by precipitation with small amounts of a 2 M sodium phosphate solution made by mixing the monobasic dihydrogen phosphate and dibasic monohydrogen phosphate forms.

Cell-permeabilization experiments

To demonstrate lysenin's capabilities to control cell membrane permeability via pore formation, we utilized Jurkat and ATDC5 cell lines.

Jurkat cells (American Type Culture Collection), kindly provided by Dr. Denise Wingett at Boise State University, were grown in RPMI-1640 media (Sigma-Aldrich) supplemented with 10% fetal bovine serum (FBS, Atlanta Biologica), 1% penicillin/streptomycin, 1.5 g/L sodium bicarbonate, 4.5 g/L D-(+) glucose, 10 mM HEPES, 1 mM sodium pyruvate, and 2 mM L-glutamine. Cells were grown at 37^{o}C and 5% CO_2, and passaged before reaching a cell density of ~1 x 10^6 cells/ml. On the day of experimentation, cells were counted using a bright-line hemocytometer (Hausser Scientific), washed twice with 1 ml of modified 1X HBSS (without calcium chloride, magnesium sulfate, sodium bicarbonate or phenol red, Sigma-Aldrich), centrifuged, and the cell-pellet was resuspended in 1X HBSS containing 1 µg/ml PI. One hundred µl

solution, containing ~1 x 10^5 cells were seeded per well in tissue culture treated 96 wells plate (Corning). Two sets of four wells with cells (one set for permeabilization only, and the other for chitosan blockage) underwent addition of 1 µl of 0.6 mg/ml lysenin per well. No lysenin or chitosan was added to another set of four wells included as a control in the experiment. A Biotek Synergy MX microplate reader (BioTek) was used to measure the fluorescence intensity of PI every 5 minutes for 50 minutes total duration. The measurement from all samples was taken at excitation/emission wavelength of 535/617 nm and sensitivity set at 65 at room temperature. After 20 minutes, 0.5 µl of 0.1% chitosan in 0.01 M acetic acid (25 nM final concentration) was added to one set of four wells to assess the inhibition of PI transport through lysenin channels upon blockage with chitosan.

Jurkat cell viability. In a first set of experiments, we investigated the dose-viability relationship for Jurkat cells exposed to either lysenin or chitosan by using the Alamar Blue (resazurin) assay [60]. Jurkat cells were resuspended in either modified 1X HBSS or complete Jurkat medium (89% RPMI-1640 medium, 2 mM L-glutamine, 10 mM HEPES, 1 mM sodium pyruvate, 4.5 g/l D-(+)-glucose, 1.5 g/l sodium bicarbonate, 10% FBS, and 1% penicillin/streptomycin) at ~5 x 10^5 cells/ml and 0.2 ml of the cell suspension was seeded into flat-bottom 96 well plates. The cells were rested at 37 °C and 5% CO_2 for 30 minutes, then treated in the same conditions with either lysenin (0 – 500 nM) for 30 minutes, or chitosan (0 – 250 nM) for 20 hours. Resazurin solution (10% (v/v) was added to each sample for an additional 4 hour incubation period at 37 °C and 5% CO_2. The reduction of the blue, non-fluorescent resazurin to fluorescent resorufin in viable cells was measured by using the Biotek Synergy MX microplate reader at 530 nm

(excitation) /590 nm (emission). The percent viability for each treatment was calculated as percentage of untreated controls.

ATDC5 cells, kindly provided by the Biomolecular Research Center at Boise State University, were grown in GIBCO® Dulbecco's modified Eagle's medium: nutrient mixture F -12 (DMEM/F12) supplemented with 5% FBS and 1% penicillin/streptomycin. Cells were grown until they reached a confluency of 70-80%, after which they were trypsinized for 7-9 minutes with 0.25% trypsin-EDTA. The enzyme was deactivated by the addition of 7 ml of medium. The cells were counted using the hemocytometer, centrifuged, and resuspended in fresh media before seeding in a tissue culture-treated 75 cm^2 flask (VWR International) at cell densities of either ~1 x 10^5 cells/ml or ~0.5 x 10^5 cells/ml. The cells were grown and maintained at 37ºC and 5% CO_2.

For ATDC5 cell permeabilization experiments, two ml of ~1 x 10^5 cells/ml were seeded in 35 mm glass bottom culture dishes (GBCD) with 10 mm microwell (MatTek Co). Cells were incubated at 37ºC and 5% CO_2 for ~24 hours. ATDC5 cell membrane permeabilization via lysenin channels was imaged and assessed by using a Zeiss LSM 510 Meta confocal system with the Zeiss Axiovert Observer Z2 inverted microscope and ZEN 2009 imaging software (Carl Zeiss, Inc., Thornwood, NY). Images were acquired in a single plane utilizing the Plan-Apochromat 20x/NA 0.80 or Fluar 40x/NA1.30 oil objectives and with Argon (488 nm) and HeNe (543 nm) laser sources. Fluorescence was detected using a 500 – 550 nm band-pass for calcein and a 590 long-pass filter for PI/Alexa 546-phalloidin (Thermo Fisher), respectively.

On the day of experimentation, one day-old cell cultures in GBCD were washed twice with 1 ml of modified 1X HBSS, followed by addition of 200 µl of 2 µM calcein-

AM (Thermo Fisher) to estimate cell-viability. Permeabilization was monitored upon simultaneous addition of 100 µl of 1 µg/mL of PI solution containing 1 µl of 0.17 µg/µl of lysenin monomer.

To determine the loading of cell-impermeant phalloidin conjugated with Alexa-546, cells were washed twice with 1 ml of 1X HBSS followed by the addition 100 µl of 1X HBSS to each microwell. One µl of 0.6 µg/µl lysenin was added to the cell solutions and incubated for ~10 minutes at room temperature. Cells were washed twice with 1 ml of 1X HBSS to remove the free lysenin from the bulk solution, and 100 µl of Alexa Fluor® 546 Phalloidin working solution added for permeabilization imaging by confocal microscopy. A stock solution of Alexa Fluor® 546 Phalloidin was prepared by dissolving 300 units in 1.5 ml pure methanol. The working solution was prepared by diluting the 50 µl of stock solution in 1 ml of 1X HBSS.

ATDC5 cell viability. To investigate the combined influence of dyes, blockers, and lysenin on the viability of ATDC5 cells, we based our approach on the widely-used PI/calcein-AM double staining assay. However, we accounted for the fact that non-permeant dyes may gain access to the cytosol upon membrane permeabilization by lysenin. Cell preparation experiments similar to the permeabilization studies (*vide supra*) were employed for viability assessment in the presence of phalloidin. The cells were exposed to the non-permeant dye by addition of 100 µl of Alexa Fluor® 546 phalloidin working solution and permeabilized with 1 µl of 0.6 µg/µl lysenin. After 10 minutes incubation, the free lysenin and phalloidin were removed by washing twice with 1X HBSS. The media in the wells was completed by addition of 2 ml DMEM/F12. After 5 hours of incubation at 37^{o}C and 5% CO_2 the cells were washed, rendered fluorescent by

addition of 100 µl of 2 µM calcein-AM, and imaged by confocal microscopy for combined permeabilization/viability assessments.

Results and Discussion

Controlled permeabilization of planar bilayer lipid membranes

The conductance state of lysenin channels inserted into membranes is greatly dependent on the influences exerted by chemical and physical stimuli such as transmembrane voltage, ligands, temperature, or blockers [41, 52-55, 57]. The objective of gaining acquired control over the membrane permeability via conductance modulation requires careful selection of the chemicals used as conductance controllers to minimize undesired interferences with the membrane system under consideration. The reversible blockage of lysenin channels by a ligand-gating mechanism triggered by multivalent ions is well documented [54, 55]. Trivalent lanthanide cations along with Al^{3+} ions are the most effective inhibitors of the macroscopic conductance of lysenin channels [54, 55]. In addition, the conductance properties of the membrane are fully reinstated (i.e, the channels re-open) after inhibitor removal by chelation or precipitation [54, 55]. The use of multivalent ions may be appropriate for reversibly controlling the transport in artificial membrane systems, and studies presented later in this thesis support this assertion. However, some multivalent ions may induce toxicity upon interacting with living systems [61, 62]. Therefore, we explored alternative approaches for controlling the membrane permeability, and tested potential interferences between the channels and the various biochemical/biological components introduced in the experimental system. Initial experiments focused on exploring lysenin conductance modulation by ATP in artificial membrane systems since ATP may be released from photolabile cages [56]. Exposure of

planar lipid membranes containing lysenin channels to increasing amounts of ATP showed a concentration-dependent inhibition of the macroscopic conductance [63] (Figure 2a). The changes were completely reversible as indicated by conductance recovery upon ATP removal by buffer exchange (Figure 2b).

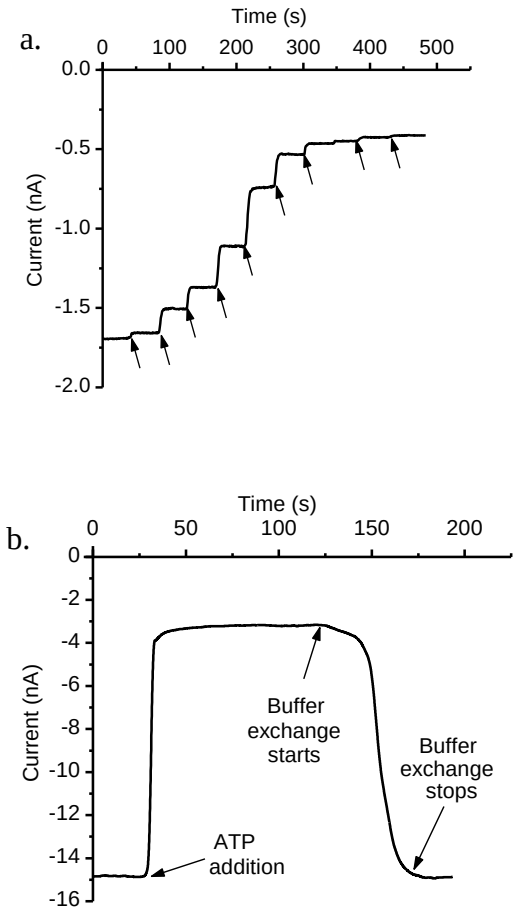

Figure 2. ATP reversibly inhibits the macroscopic conductance of lysenin channels. a) Successive addition of 1 mM ATP (as shown by arrows) to the solutions bathing the membrane induced a concentration-dependent inhibition of the ionic currents. b) The ionic current through the lysenin channels rapidly decreased by ~80 % upon addition of 20 mM ATP, and quickly reinstated after buffer exchange. Both experiments were recorded at -60 mV transmembrane potential in 135 mM KCl, 20 mM HEPES, pH 7.2. (With permission of Springer, Byrant et al. (2016) [63])

These results, while encouraging, suggest that the use of ATP as reversible channel blocker in either artificial or natural membrane systems is not an optimal choice.

The amount of ATP needed to induce a significant decrease in lysenin-induced permeability is relatively large. In addition, even for the highest ATP concentration used in our studies, 20 mM, the macroscopic conductance decreased by less than 80%, indicative of an incomplete resealing of the membrane. A leaky membrane may contribute to rapid dissipation of the electrochemical gradient, leading to cell death. Also, living cells are continuously producing ATP; although the average intracellular ATP concentrations (in the low mM range) [64], are under the levels required for a significant reduction in conductance, uncontrolled changes in its concentration may diminish the ability to precisely control membrane permeability by affecting lysenin's conducting state. Therefore, our subsequent studies considered irreversible blockage of lysenin channels by chitosan. Chitosan is a poly-cationic and bio-inert molecule that acts as an efficient blocker of lysenin channel conductance purportedly by a trap and lock mechanism [57]. However, earlier experiments were performed in planar BLMs bathed by simple electrolyte solutions containing only KCl and buffer [57], and our preliminary experiments employing live cells indicated that simple formulations are not compatible with cell survival even for limited time exposures. Exposure of live cells to 1X HBSS, for a short time, improved cell survival, but no study describes chitosan inhibition efficacy in complex buffers to our knowledge. Consequently, we performed macroscopic conductance measurements on lysenin channels inserted into planar BLMs using 1X HBSS as the support electrolyte. Addition of 5 µl of 0.1% chitosan to the support electrolyte (25 nM final concentration) under continuous stirring and at -60 mV bias potential induced a rapid and significant decrease (larger than 99%) of the macroscopic ionic current, confirming that channel blockage may occur in this particular electrolyte

solution (Figure 3). Buffer exchange did not reinstate the macroscopic conductance, and we concluded that the induced changes were irreversible, as previously reported for simpler electrolyte solutions [57].

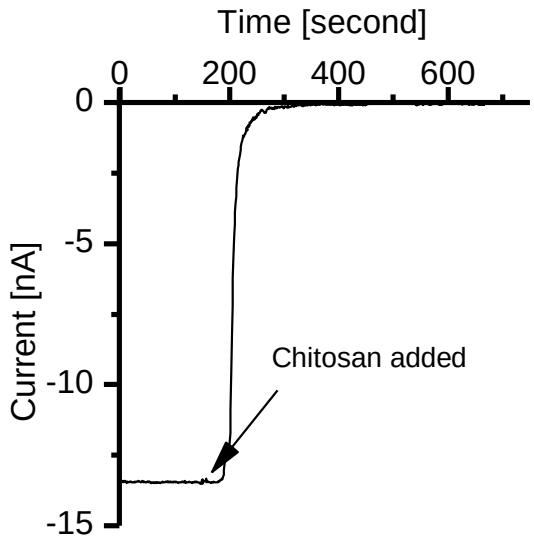

Figure 3. Chitosan inhibits the transport properties of lysenin channels in complex buffers. Addition of 25 nM chitosan yielded a complete reduction of the ionic currents at -60 mV bias potential in 1X HBSS.

Next, we asked whether the fluorescent dyes intended for analysis of membrane permeabilization would interact with lysenin channels and modulate their conductance. Many dual color dye pairs for assessing cell permeabilization and status (i.e., live/dead) use non-permeant intercalating dyes, which undergo increases in fluorescence after binding to nucleic acids [65-68], and permeant AM dyes (ester forms), which become fluorescent after hydrolytic attack from esterases present in the cytoplasm of living cells. Our first attempt to introduce the intercalating EtHD dye into Jurkat cells failed (no significant nuclear staining occurred), suggesting that lysenin may not support transport of this dye into cytosol. In order to decipher the molecular basis of this phenomenon, we performed voltage clamp experiments by employing lysenin channels inserted into planar

BLMs and exposed to KCl-based electrolyte solutions. Successive additions of EtHD (final concentration 1.63 μM, and 6.29 μM, respectively) yielded an almost complete annihilation of the macroscopic conductance, as indicated by the sustained decrease of the ionic current at -60 mV bias potential (Figure 4a). Such dramatic influence of EtHD on lysenin's conductance may explain the observed inability of the dye to cross the membrane of live cells permeabilized with lysenin, thus preventing access to the nucleus. The mechanism of channel blockage by EtHD is unknown but based on our previous work on lysenin inhibition we assume that electrostatic interactions are responsible for either channel occlusion or that EtHD acts by triggering a ligand-gating mechanism [54, 55].

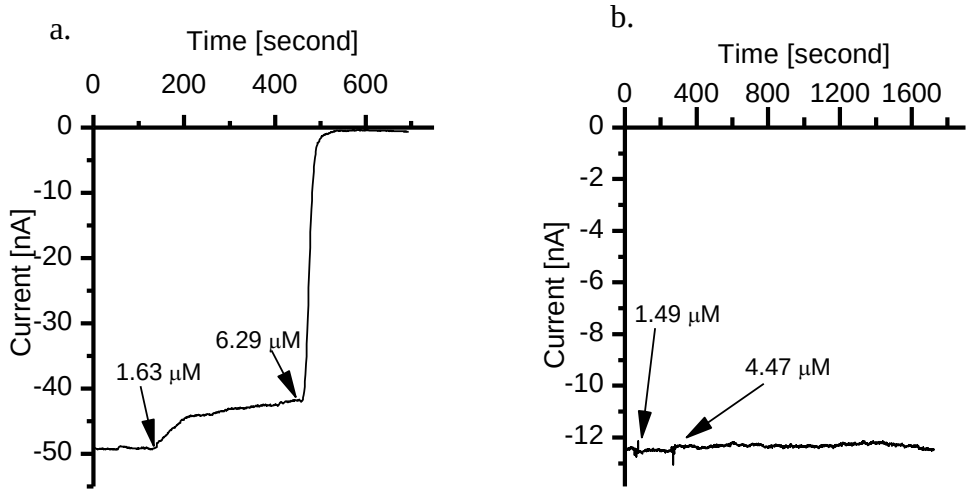

Figure 4. Lysenin channel conductance modulation by intercalating agents. a) EtHD reduced the macroscopic ionic currents through lysenin channels b) PI addition elicited negligible changes in the macroscopic currents. Both experiments were performed in 135 mM KCl, 20 mM HEPES, pH 7.2, and at -60 mV transmembrane voltage. The additions and final concentrations of the intercalating agents are indicated by arrows.

Whatever the origin of the observed blockage, EtHD was not considered suitable for controlled permeabilization studies. In contrast, addition of similar amounts of PI produced only negligible changes in the ionic current (Figure 4b), suggesting the absence

of specific or non-specific interactions with the channels. Like EtHD, PI acts as a non-permeant intercalating agent, and is often used in combination with other AM dyes for transport and cell status (live/dead) assessment [69, 70]. PI is also one of the most used dyes for studies on transport through transient pores generated with laser pulses during optoporation [71-73], and PI may cross membranes through pores larger than 1.5 nm [74]. Consequently, we concluded that PI is the optimal choice for further studies on cell membrane permeabilization with lysenin channels. All the other dyes used in this work are: calcein, calcein-AM, and phalloidin, showed no changes in microscopic conductance of lysenin channels when added to the bulk solutions at concentrations similar to what was used for live cell experiments (*data not shown*).

Liposome loading via lysenin channels

To demonstrate that lysenin channels may facilitate the entrapment and release of non-permeant molecules we conducted experiments using liposomes. Multivalent ions were used to control the channel conducting state of lysenin, and therefore the membrane permeability. Non-permeant calcein was used as a model molecule to assess loading into, and release from, liposomes by fluorescence spectroscopy or microscopy. Also, given their ability to quickly and reversibly shut down lysenin's conductance by a ligand-gating mechanism [54, 55], Al^{3+} cations were utilized in these experiments. It is worthy to note that this approach provided an opportunity to simplify the procedure of assessing lysenin-mediated loading. While unincorporated calcein may be removed by classic separation techniques such as dialysis, chromatography, or centrifugation, we used a distinctive property of calcein, i.e. the fluorescence quenching by multivalent metal ions [75]. This property enabled the elimination of external fluorescence to render the loaded liposomes

fluorescent against the background. While a previous report shows that Al^{3+} is among the most potent multivalent ion for inhibition of the macroscopic conductance of lysenin, no consistent report have determined the quenching effects of Al^{3+} on calcein. Our exploration indicates that the addition of Al^{3+} cations to a 50 µM calcein solution strongly quenched the fluorescence in a concentration-dependent manner (Figure 5). In addition, fluorescence quenching occurred at concentrations larger than what is needed to efficiently inhibit the macroscopic conductance of lysenin channels (which is ~ 25 µM [54, 55]. The present work exploited this feature to reduce the background fluorescence by adding quenching multivalent cations to the liposome mixture, assuming that these ions would rapidly close the channels and quench only the unincorporated calcein. Once resealed, it was anticipated that the sealed membrane would protect the entrapped dye from quenching.

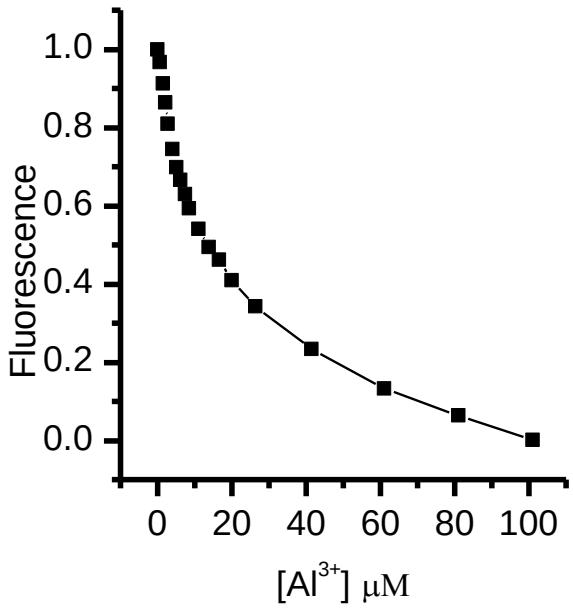

Figure 5. Al3+ effectively quenches the fluorescence of calcein in a concentration-dependent manner. Successive addition of Al3+ ions induced a progressive decrease of the relative fluorescence of 50 µM calcein (λex = 485 nm, λem = 520 nm).

Wide-field microscopy indicated the presence of uniform and well dispersed liposomes in the sample solution after extrusion (Figure 6). Spherical membrane permeabilization was performed by vigorously mixing 50 µl liposomes with 1 µl of 0.3 µM lysenin at room temperature. Microscopy imaging performed on the sample after permeabilization provided images similar as Figure 6 and indicated the absence of aggregation.

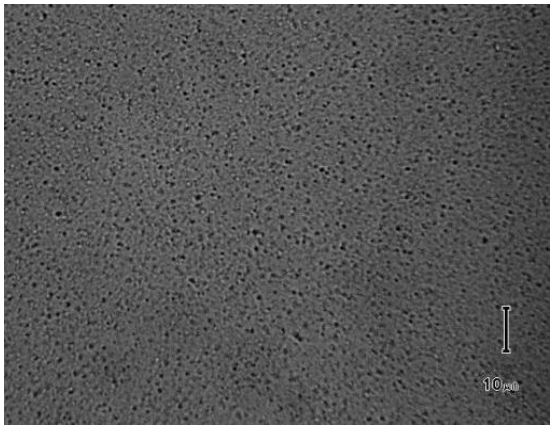

Figure 6. Well dispersed and uniform liposomes produced by extrusion. Liposomes solution produced from lipid mixtures of Aso, Chol, and SM lipid mixtures yield uniformly distributed and well dispersed liposomes.

After addition of calcein (50 µM final concentrations) to the solution containing permeabilized liposomes, the sample was left to equilibrate for six hours at room temperature in a dark container, and then microscopy images were taken. Non-fluorescence imaging showed intact liposomes in solution (Figure 7a). The lack of fluorescence from the individual liposomes demonstrated that the fluorescent dye did not accumulate at the membrane surface or into the intra-membrane space (Figure 7b).

a. b.

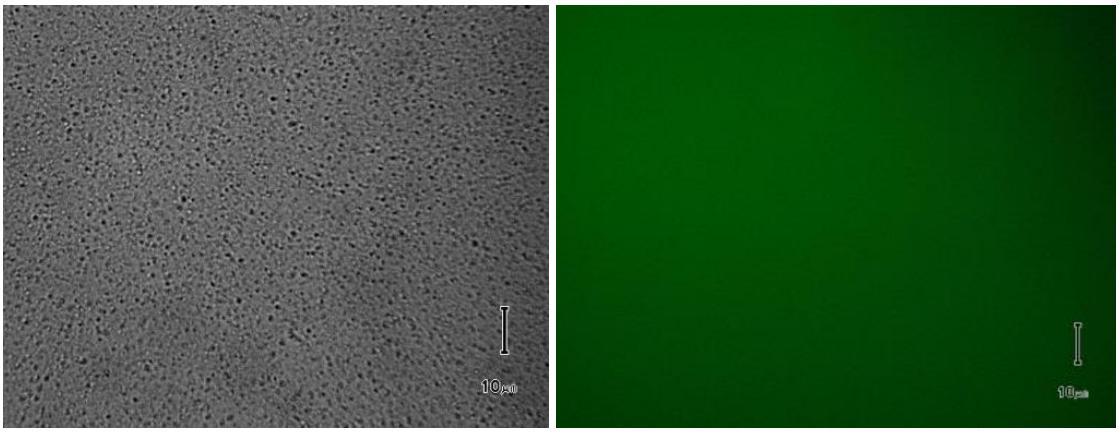

Figure 7. Liposomes treated with lysenin and calcein are uniform and well dispersed. a) Transmitted light imaging showing intact liposomes in solution after permeabilization and calcein addition. b) No fluorescent liposomes have been observed after calcein addition to the solution of liposomes containing open lysenin channels in the membrane.

The liposome membranes were resealed by addition of 100 μM Al^{3+} to the mixture, which blocked the transport through the lysenin channels, trapped the calcein inside liposomes, and quenched the non-loaded dye. Fluorescence microscopy images taken one hour after addition of Al^{3+} (50 μM final concentration) revealed highly-fluorescent liposomes and indicated their successful loading and resealing (Figure 8a). We observed that not all the liposomes incorporated the dye by switching the illumination from fluorescence to visible-transmitted light conditions. Although such effect could be a result of incomplete resealing upon Al^{3+}addition, the most reasonable explanation relies on the fact that not all of the large liposomes produced by extrusion were unilamellar. Lysenin may interact with multilamellar structures, but it cannot be assumed that the inserted pores will completely penetrate thick multilayered structures to create a conducting pathway between the inner water-filled cavity and the external solution. Next, the release of the incorporated calcein was performed by precipitating the Al^{3+} cations with 10 mM phosphate added directly to the liposome solution. A fluorescence image taken 20 minutes after precipitation showed no fluorescent liposomes

(Figure 8b). However, transmitted-light imaging showed intact liposomes like those shown in Figure 7a, confirming dye leakage through the lysenin channels that reopened after phosphate-removal of the inhibiting Al^{3+} cations.

a.

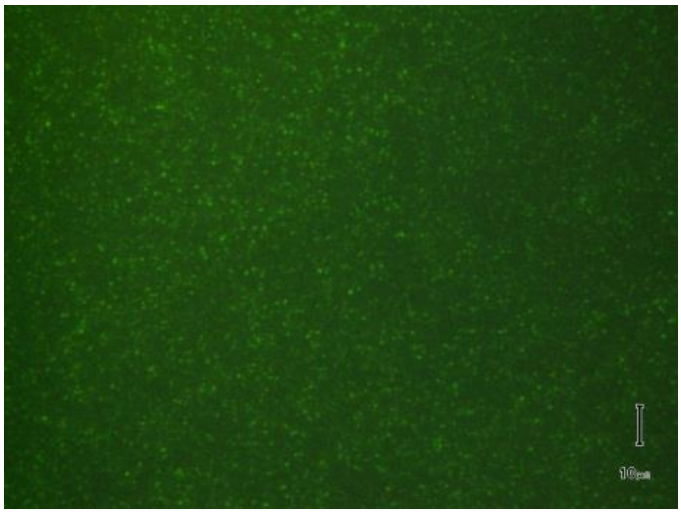

b.

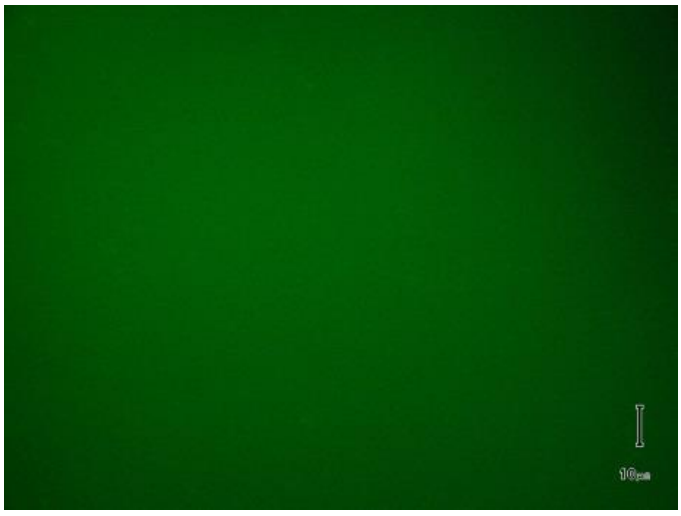

Figure 8. Al3+ ions control the lysenin-induced permeability in liposome membranes. a) Addition of Al3+ blocked the lysenin's conductance, trapped the calcein inside, quenched the non-entrapped calcein and rendered the liposomes fluorescent against the background. b) Addition of 10 mM phosphate buffer yielded Al3+precipitation, channel reopening, and a homogeneous distribution of the dye inside and outside of liposomes. The liposomes were not anymore observed as individual fluorescent structures.

Cell-permeabilization of Jurkat and ATDC5 via lysenin channels

Viability of Jurkat cells after treatment with lysenin or chitosan. The overall goal of a versatile and efficient approach for gaining temporary control over cell membrane permeability, while maintaining overall viability, raises the question whether lysenin or blockers, such as chitosan, may induce cell death at concentrations required for membrane permeabilization or reseal. To address this question we employed viability tests on Jurkat cells in the presence of variable concentrations of either lysenin or chitosan. The Alamar Blue (resazurin) assay test showed that Jurkat cell viability decreases with the concentration of lysenin in the 0 – 500 nm range (Figure 9). This experiment demonstrates the lethal effects of lysenin on Jurkat cells, which is expected since lysenin introduces large conducting pathways that may disperse the electrochemical gradient and lead to cell death. Nonetheless, the maximum concentration of lysenin used in the viability study (500 nM) is a few times greater than the concentration used for permeabilization studies, which is ~180 nM. Although Jurkat cell viability systematically decreased with concentration, a viability rate of ~20% was estimated even for the highest lysenin concentration, 500 nM. This result indicates that lysenin may be used for permeabilization while preserving viability within reasonable rates for transfection experiments [76, 77]. The next experiment addressed Jurkat cells viability upon exposure to chitosan. The viability data (Figure 10) showed that chitosan has negligible effects on cell survival using concentrations one order of magnitude higher than what is required to efficiently block the lysenin channels, i.e 25 nM in artificial membrane systems (see Figure 3).

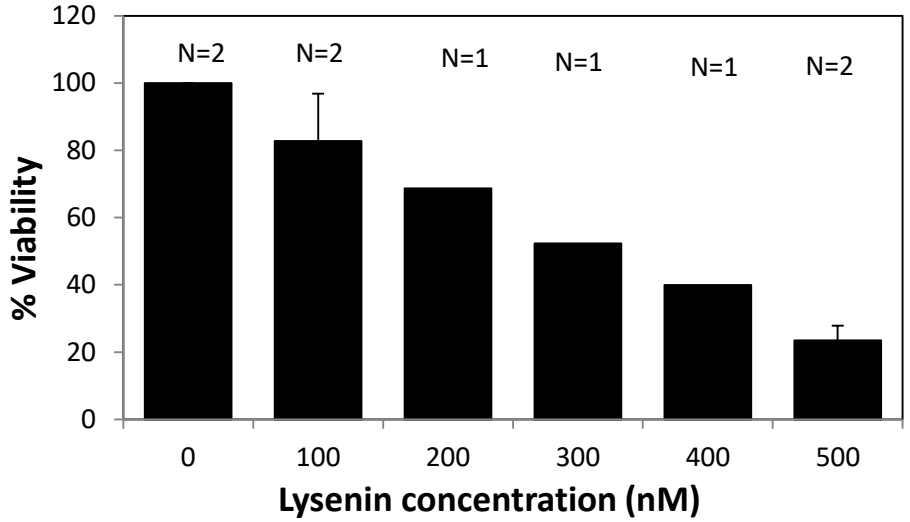

Figure 9. Lysenin affects Jurkat cell viability in a concentration dependent manner. Cell viability decreases with lysenin concentration in the range 0-500 nM. (N = 1-2)

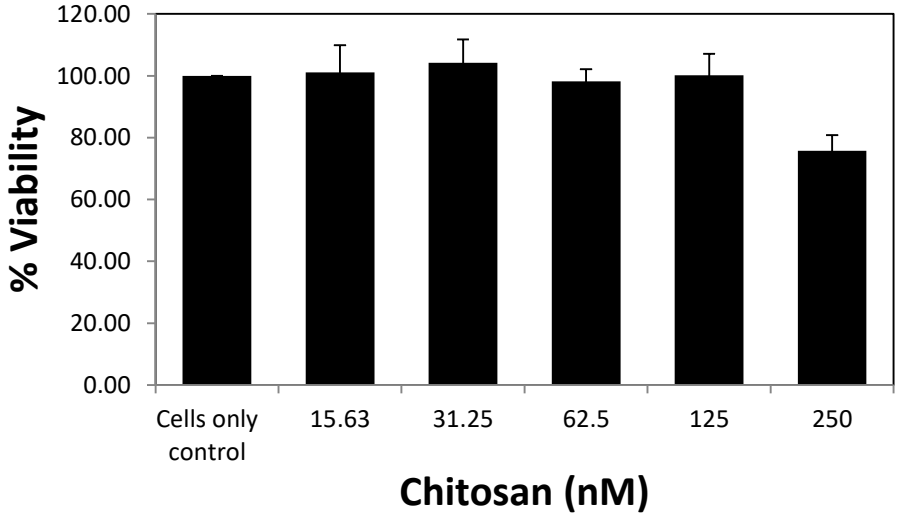

Figure 10. Chitosan has limited effects on Jurkat cell viability. Cell-viability measured 20 hours after incubation at different concentrations of chitosan (0 – 250 nM) demonstrated no significant effect on cell-viability until 250 nM. The highest chitosan concentration used (250 nM) yielded a ~20% decrease in viability. (mean ± SD, n = 3)

Chitosan control of the transport of membrane impermeant PI into Jurkat cells

PI's fluorescence undergoes a large hyperchromic shift upon intercalation between the stacked bases of DNA molecules, which may be used as indicator of the dye

transport through the cell membrane. However, the membrane of living cells constitutes a natural barrier that prevents PI crossing. Therefore, in live Jurkat cells, the PI may cross the membrane only if the transport is mediated by transporters (such as lysenin channels) present in the membranes. Our viability data have shown that neither lysenin nor chitosan significantly affects Jurkat cell viability at the concentrations required by permeabilization experiments. However, a demonstration of chitosan's ability to effectively control the transmembrane transport is needed. To fill this gap, we used Jurkat cells permeabilized with lysenin in the presence of PI and analyzed the evolution of nuclear staining in the absence of chitosan at specified times after lysenin addition. As shown in Figure 11, the absence of lysenin from the control samples (-lysenin, -chitosan, + PI) elicited a steady low fluorescence, indicating that the dye did not cross the membrane of live cells. In contrast, in the presence of lysenin, PI diffused into the cytosol and stained DNA in the nucleus, which was observed as a gradual increase in the fluorescence intensity. Similarly increasing fluorescence was observed before chitosan addition in the samples intended for assessing controlled permeability by chitosan. Nonetheless, chitosan addition at 20 minutes prevented further diffusion of the dye (as observed from the steady fluorescence), confirming that the transmembrane transport of PI was stopped. The increase in fluorescence observed for the first point recorded after chitosan addition may be explained by the PI still present in the cytosol but not yet diffused into the nucleus. These studies support the conclusion that chitosan addition prevented further PI transport by blocking the lysenin channels.

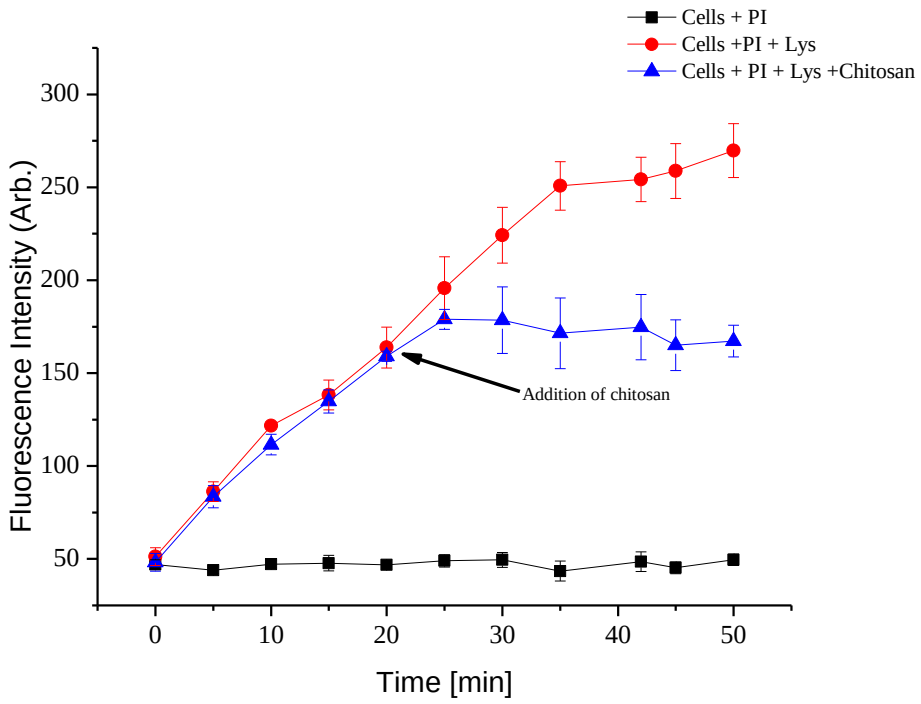

Figure 11. Chitosan is effective in controlling the transport of PI across the cell membrane in Jurkat cells. PI entrance via lysenin channels was assessed from the PI fluorescent intensity. Addition of chitosan 20 minutes after the initiation of permeabilization stabilized the fluorescent intensity (triangles). In contrast, continual increase of fluorescence was measured for the unblocked lysenin channels (circles). In the absence of lysenin, PI did not cross the cell membrane (squares). The steady line obtained in the absence of lysenin is indicative of membrane integrity. (mean ± SE, n = 4)

ATDC5 cells permeability and viability

To simultaneously assess the efficiency of lysenin-induced permeabilization and cell viability we employed the live/dead staining technique comprising the use of calcein-AM/PI pair. Calcein-AM has a weak fluorescence signal in the ester form but its lipophilic character renders it membrane-permeant. In the cytoplasm of living cells, the dye is converted to the highly fluorescent calcein form by the hydrolytic activity of active esterases, therefore cell viability is indicated by sustained green fluorescence. In contrast, PI is non-permeant through the membranes of viable cells, but it may pass through

membranes with impaired transport (i.e, dead cells or permeabilized membranes). However, both dyes may cross the membrane through lysenin channels inserted into viable cells membrane, and this feature was used for simultaneous analysis of permeability and viability. The viability of untreated ATDC5 cells was estimated by confocal microscopy in the presence of calcein-AM (Figure 12a). A succession of images taken at different time intervals after membrane permeabilization by lysenin in the presence of PI (Figure12, b-f) showed the development of a red color that increased with time. This evolution may be explained by the passage of PI through lysenin channels and further staining of the nucleus. However, the green fluorescence persisted, suggesting that many cells maintained viability. As time elapsed, some red-stained cells presented reduced or no green fluorescence, which was considered indicative either of cell death due to prolonged exposure to lysenin or excess of loaded PI.

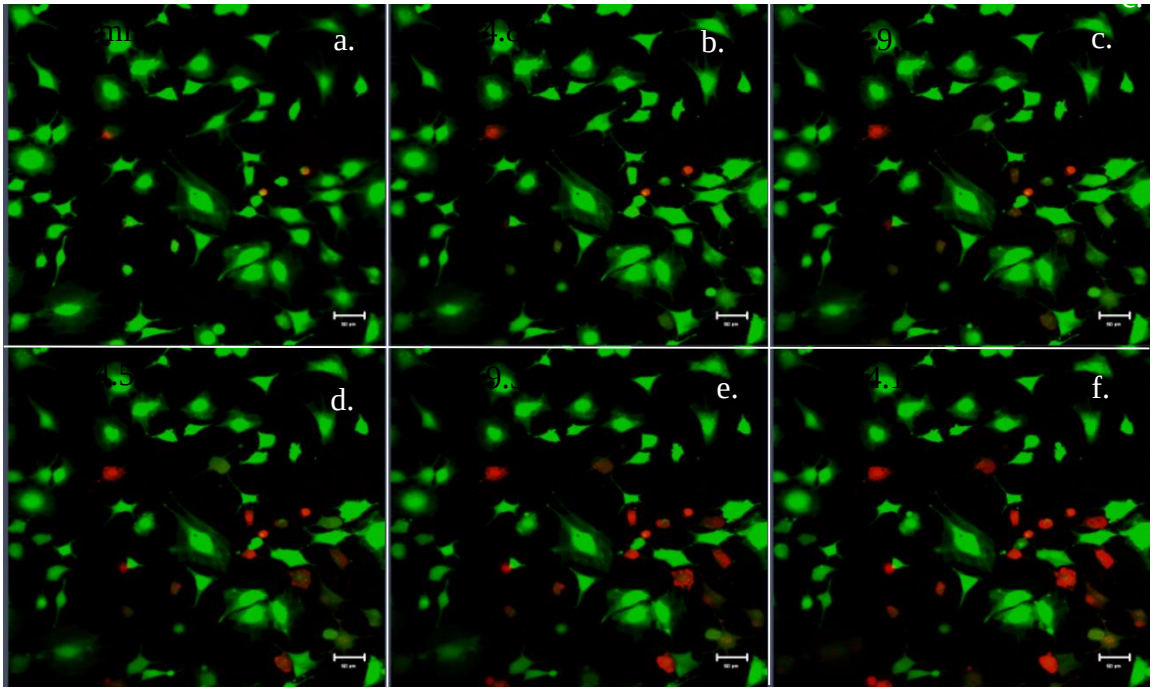

Figure 12. Lysenin is able to permeabilize adherent ATDC5 cells and allow PI uptake. Time evolution of PI uptake into ATDC5 cells permeabilized with lysenin channels. The cells were simultaneously stained with permeant calcein-AM (green fluorescence) and non-permeant PI (red fluorescence). Scale bars: 50 µm

Transport of cell-impermeant phallodin in ATDC5 via lysenin channels

Our explorations on lysenin-induced permeabilization in ATDC5 cells continued by investigating the mediated transport of phalloidin, a bicyclic heptapeptide toxin from the poisonous mushroom *Amanita phalloides* [78]. With the well-known exception of hepatocytes, which readily take it up through an unknown mechanism, phalloidin is membrane non-permeant. Once transported into the cytosol, phalloidin binds to filamentous-actin (F-actin) with high affinity, thereby preventing the depolymerization of actin fibers [79-82]. The specific tagging of phalloidin with dyes that fluoresce only upon binding to F-actin evolved into powerful methods of actin filaments investigations [83-86]. However, these procedures require access to the cytosol, which may be achieved by microinjection, optoporation, or transfection [11, 29, 87]. To simplify the experimental

approach, we propose the use of lysenin for introducing cell-impermeant phalloidin into adherent ATDC5 cells. Cells grown in 35 mm culture dishes for 24 hours, incubated with lysenin for ~ 8-10 minutes, and subsequently washed, have been exposed to Alexa-546® phalloidin conjugate. An otherwise similar control experiment comprised the addition of Alexa-546® phalloidin conjugate without the intermediate step of lysenin-induced permeabilization. After cell identification in the well by transmitted light microscopy (Figure 13a), confocal microscopy analysis showed that the lysenin-treated samples developed the characteristic red fluorescence, hence confirming phalloidin passage through the membrane and F-actin attachment (Figure 13b). In contrast, the control sample containing phalloidin treated cells that were not previously exposed to lysenin showed no characteristic red fluorescence (See Figure 14b), confirming that phalloidin is able to cross the membrane barrier only through open lysenin channels.

a. b

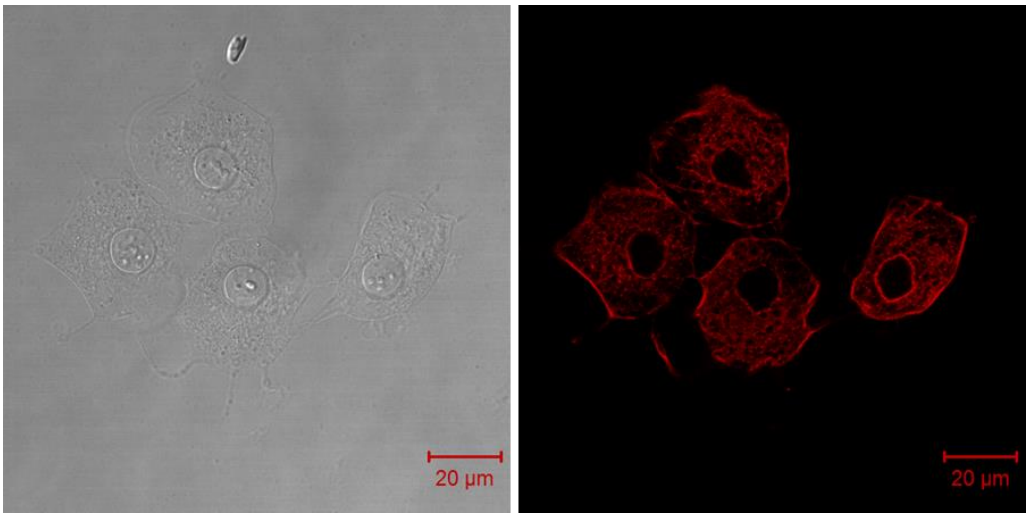

Figure 13. Lysenin channels allow the transport of membrane-impermeant phalloidin across the cell-membrane. a) The transmitted light image showing the presence of cells and (b) the fluorescence image showing the presence of intracellular phalloidin after lysenin treatment. Scale bars: 20 µm

ATDC5 cell viability after loading phalloidin via lysenin channels. Lysenin is a cytolytic pore forming toxin and phalloidin may exert toxicity effects by inhibiting the depolymerizaton of F-actin, hence their conjugate actions may affect cell viability. To examine the potential combined lethal effects, we used calcein-AM as a live indicator in conjunction with Alexa Fluor 546 phalloidin as permeability tracer for lysenin permeabilized, and non-permeabilized (control) ATDC5 cells. The cells incubated with lysenin and Alexa Fluor 546 phalloidin for ~ 10 minutes and analyzed by confocal microscopy showed bright red staining of actin filaments, indicative of permeabilization (Figure 14 a (i)). However, the negative control cells (-lysenin, + Alexa Fluor 546 phalloidin) did not show the characteristic red fluorescence in otherwise identical conditions, demonstrating that untreated membranes do not allow phalloidin passage (Figure 14 b (i)). Next, lysenin-exposed cells and control cells were incubated in DMEM/F12 for ~ 5 hours, and calcein-AM added for viability assessments. Both lysenin-

permeabilized and non-permeabilized ATDC5 cells showed the green fluorescence, indicative of live cells at this time point. (Figures 14 a (ii) and b (ii)).

a.

b.

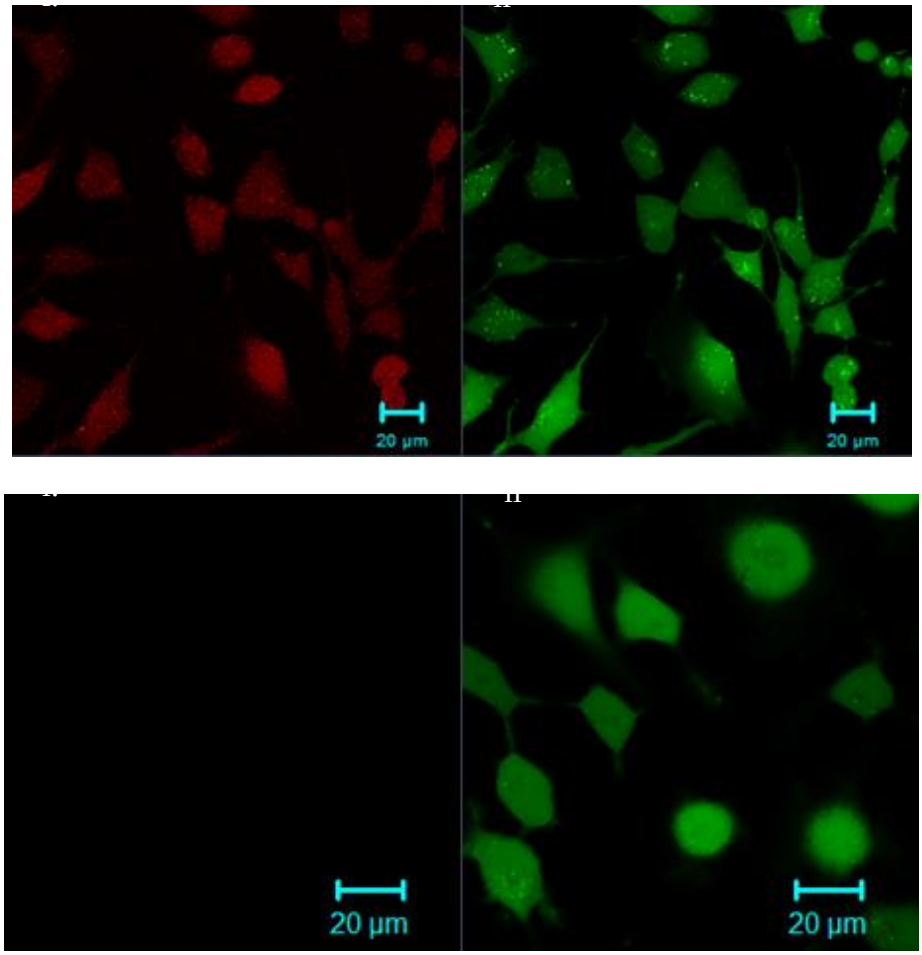

Figure 14. The phalloidin loaded, lysenin-permeabilized ATDC5 cells remain viable after 5 hours. a) Lysenin-permeabilized cells allowed (i) phalloidin loading , (ii) and calcein-AM fluorescence indicated cell-viability after incubation in DMEM/F12 media for 5 hours. b) The lysenin-free control showed (i) the absence of phalloidin, while (ii) calcein-AM fluorescence indicated cell-viability in otherwise similar conditions.

Conclusions and Perspectives

Our studies provide evidence that lysenin channels may be used to gain control over the permeability function of artificial and natural cell membranes. The employment of liposomes as model lipid membranes allowed reversible control of molecular transport

through lysenin channels using Al^{3+} cations as inhibitors of conductance. In addition, cation removal by precipitation reinstated the macroscopic conductance and high membrane permeability. Two distinct cell lines, Jurkat and ATDC5, respectively, were employed for lysenin-mediated permeabilization studies, in conjunction with viability assessments. Successful loading of macromolecules such as dyes and bicyclic peptides through lysenin channels inserted into membranes, while maintaining cell viability, supports the applicability of this approach to temporary cell membrane permeabilization. Lysenin's pore-formation mechanism requires the presence of SM in the target membrane, which could be considered a limiting factor for wide applicability. However, SM may be easily introduced in artificial membrane systems, and SM is also a major component of all mammalian cells, therefore numerous biological systems may be explored. Lysenin has also the unique advantage of responding to multiple regulatory mechanisms, which enhance the control of membrane permeability. Our work on liposomes showed that multivalent cations may be used to gain advanced control over the membrane barrier function. While such advanced capabilities are critical for artificial membrane systems, their utility for live cells is not conclusive because of their potential cytotoxicity. Controlled permeability studies performed on Jurkat cells demonstrated that chitosan may be used to control the passage of PI. In addition, viability tests of this cell line showed that lysenin is not as toxic as presumed from its great cytolytic activity. In addition, our ATDC5 studies demonstrated passage of macromolecules through lysenin channels even in complex environments. These studies included viability tests and were developed without employing any control of the lysenin-induced permeability. Our results do not indicate that there was potential gating or occlusion induced by specific

components in the bulk media. An explanation for this may be that the cells used in our experiments are capable of sustaining multiple membrane lesions without facing premature death. Similar explanations have been advanced for streptolysin, a potent pore forming toxin proposed to be used for cell permeabilization, for which no regulatory mechanism is known [88, 89]. However, regulatory mechanisms are important, as the ability to switch on/off membrane permeability may prove crucial for cells which are highly sensitive to electrochemical gradients, such as muscle or nerve cells. In conclusion, our studies open novel avenues for controlling the permeability of artificial and natural cell membranes, which may find applicability in controlling crucial biological functionalities, development of smart bioreactors encased in lipid vesicles for enzymatic reaction, advanced systems for controlled drug delivery, or the development of artificial cells.

References

1. Aidley, D.J. and P.R. Stanfield, *Ion channels. molecules in action*. 1996, Cambridge: Cambridge University Press.

2. Andersen, O.S., H.I. Ingolfsson, and J.A. Lundbaek, *Ion channels.* Wiley Encyclopedia of Chemical Biology, 2008: p. 1-14.

3. Ashcroft, F.M., *Ion channels and disease*. 1999, San Diego, CA, USA: Academic Press.

4. Baruscotti, M., G. Thiel, and A. Moroni, *Ion transport in biological membranes,* in *Encyclopedia of Condensed Matter Physics*, G. Bassani, G. Liedl, and P. Wyder, Editors. 2005, Elsevier.

5. Bezanilla, F., *Voltage-Gated Ion Channels.* IEEE Transactions on Nanobioscience, 2005. **4**(1): p. 34-48.

6. Bezanilla, F., *How membrane proteins sense voltage.* Nature Reviews Molecular Cell Biology, 2008. **9**: p. 323-332.

7. Hille, B., *Ion channels of excitable membranes, Third edition*. 2001, Sunderland, MA: Sinauer Associates, Inc.

8. Wong, F.K., et al., *Microinjection of membrane-impermeable molecules into single neural stem cells in brain tissue.* Nature Protocols, 2014. **9**(5): p. 1170-1182.

9. Neumann, E., et al., *Gene transfer into mouse lyoma cells by electroporation in high electric fields.* The EMBO Journal, 1982. **1**(7): p. 841-845.

10. Hapala, I., *Breaking the barrier: methods for reversible permeabilization of cellular membranes.* Critical Reviews in Biotechnology, 1997. **17**(2): p. 105-122.

11. Dhakal, K., B. Black, and S. Mohanty, *Introduction of impermeable actin-staining molecules to mammalian cells by optoporation.* Scientific Reports, 2014. **4**. doi: 10.1038/srep06553

12. Zabner, J., *Cationic lipids used in gene transfer.* Advanced Drug Delivery Reviews, 1997. **27**(1): p. 17-28.

13. Zhang, G., et al., *A cationic lipid for rapid and efficient delivery of plasmid DNA into mammalian cells.* Biochemical and Biophysical Research Communicaions, 1997. **236**(1): p. 126-129.

14. Bechara, C. and S. Sagan, *Cell-penetrating peptides: 20 years later, where do we stand?* FEBS Letters, 2013. **587**(12): p. 1693-1702.

15. Varkouhi, A.K., et al., *Endosomal escape pathways for delivery of biologicals.* Journal of Controlled Release, 2011. **151**(3): p. 220-228.

16. Cabiaux, V.r., *pH-sensitive toxins: interactions with membrane bilayers and application to drug delivery.* Advanced Drug Delivery Reviews, 2004. **56**(7): p. 987-997.

17. Majd, S., et al., *Applications of biological pores in nanomedicine, sensing, and nanoelectronics.* Current Opinion in Biotechnology, 2010. **21**(4): p. 439-476.

18. Gurnev, P.A. and E.M. Nestorovich, *Channel-Forming Bacterial Toxins in Biosensing and Macromolecule Delivery.* Toxins, 2014. **6**(8): p. 2483-2540.

19. Mura, S., J. Nicolas, and P. Couvreur, *Stimuli-responsive nanocarriers for drug delivery.* Nature Materials, 2013. **12**(11): p. 991-1003.

20. Russo, M.J., H. Bayley, and M. Toner, *Reversible permeabilization of plasma membranes with an engineered switchable pore.* Nature Biotechnology, 1997. **15**(3): p. 278-282.

21. Bhakdi, S., J. Tranum-Jensen, and A. Sziegoleit, *Mechanism of membrane damage by streptolysin-O.* Infection and Immunity, 1985. **47**(1): p. 52-60.

22. Spiller, D.G. and D.M. Tidd, *Nuclear delivery of antisense oligodeoxynucleotides through reversible permeabilization of human leukemia cells with streptolysin O.* Antisense Research and Development, 1995. **5**(1): p. 13-21.

23. Walev, I., et al., *Delivery of proteins into living cells by reversible membrane permeabilization with streptolysin-O.* Proceedings of the National Academy of Sciences, 2001. **98**(6): p. 3185-3190.

24. Teng, K.W., et al., *Labeling proteins inside living cells using external fluorophores for fluorescence microscopy.* Elife, 2017. **6**. p. e25460. doi: 10.7554/eLife.20378

25. Cisse, I., et al., *Fueling protein DNA interactions inside porous nanocontainers.* Proceedings of the National Academy of Sciences, 2007. **104**(31): p. 12646-12650.

26. Yoshimura, K., A. Batiza, and C. Kung, *Chemically charging the pore constriction opens the mechanosensitive channel MscL.* Biophysical Journal, 2001. **80**(5): p. 2198-206.

27. Kocer, A., et al., *Rationally designed chemical modulators convert a bacterial channel protein into a pH-sensory valve.* Angewandte Chemie International Edition, 2006. **45**(19): p. 3126-3130.

28. Kocer, A., et al., *A light-actuated nanovalve derived from a channel protein.* Science, 2005. **309**(5735): p. 755-758.

29. Doerner, J.F., S. Febvay, and D.E. Clapham, *Controlled delivery of bioactive molecules into live cells using the bacterial mechanosensitive channel MscL.* Nature Communications, 2012. **3**: p. 990. doi: 10.1038/ncomms1999

30. Louhivuori, M., et al., *Release of content through mechano-sensitive gates in pressurized liposomes.* Proceedings of the National Academy of Sciences, 2010. **107**(46): p. 19856-19860.

31. Ranquin, A., et al., *Therapeutic nanoreactors: combining chemistry and biology in a novel triblock copolymer drug delivery system.* Nano Letters, 2005. **5**(11): p. 2220-2224.

32. Mandal, M. and K.D. Lee. *Listeriolysin O-containing-liposome mediated cytosolic delivery of exogenous antigen*. *FASEB Journal*. 2000.

33. Mandal, M. and K.-D. Lee, *Listeriolysin O-liposome-mediated cytosolic delivery of macromolecule antigen in vivo: enhancement of antigen-specific cytotoxic T lymphocyte frequency, activity, and tumor protection.* Biochimica et Biophysica Acta (BBA)-Biomembranes, 2002. **1563**(1): p. 7-17.

34. Mandal, M., et al., *Cytosolic delivery of viral nucleoprotein by listeriolysin O-liposome induces enhanced specific cytotoxic T lymphocyte response and protective immunity.* Molecular Pharmaceutics, 2004. **1**(1): p. 2-8.

35. Mathew, E., et al., *Cytosolic delivery of antisense oligonucleotides by listeriolysin O-containing liposomes.* Gene Therapy, 2003. **10**(13): p. 1105-1115.

36. Saito, G., G.L. Amidon, and K.D. Lee, *Enhanced cytosolic delivery of plasmid DNA by a sulfhydryl-activatable listeriolysin O/protamine conjugate utilizing cellular reducing potential.* Gene Therapy, 2003. **10**(1): p. 72-83.

37. Fahrer, J., et al., *Genetically engineered clostridial C2 toxin as a novel delivery system for living mammalian cells.* Bioconjugate Chemistry, 2010. **21**(1): p. 130-139.

38. Shakor, A.-B.A., E.A. Czurylo, and A. Sobota, *Lysenin, a unique sphingomyelin-binding protein.* FEBS letters, 2003. **542**: p. 1-6.

39. Yamaji-Hasegawa, A., et al., *Oligomerization and pore formation of a sphingomyelin-specific toxin, lysenin.* Journal of Biological Chemistry, 2003. **278**(25): p. 22762-22770.

40. Bruhn, H., et al., *Dissection of the mechanisms of cytolytic and antibacterial activity of lysenin, a defence protein of the annelid Eisenia fetida.* Developmental and Comparative Immunology, 2006. **30**(7): p. 597-606.

41. Ide, T., et al., *Lysenin forms a voltage-dependent channel in artificial lipid bilayer membranes.* Biochemical and Biophysical Research Communications, 2006. **346**(1): p. 288-292.

42. Shogomori, H. and T. Kobayashi, *Lysenin: A sphingomyelin specific pore-forming toxin.* Biochimica et Biophysica Acta, 2008. **1780**(3): p. 612-618.

43. Bokori-Brown, M., et al., *Cryo-EM structure of lysenin pore elucidates membrane insertion by an aerolysin family protein.* Nature Communications, 2016. **7**. doi: 10.1038/ncomms11293

44. De Colibus, L., et al., *Structures of lysenin reveal a shared evolutionary origin for pore-forming proteins and its mode of sphingomyelin recognition.* Structure, 2012. **20**(9): p. 1498-1507.

45. Kwiatkowska, K., et al., *Lysenin-His, a sphingomyelin-recognizing toxin, requires tryptophan 20 for cation-selective channel assembly but not for membrane binding.* Molecular Membrane Biology, 2007. **24**(2): p. 121-134.

46. Kiyokawa, E., et al., *Recognition of sphingomyelin by lysenin and lysenin-related proteins.* Biochemistry, 2004. **43**(30): p. 9766-9773.

47. Kulma, M., et al., *Sphingomyelin-rich domains are sites of lysenin oligomerization: implications for raft studies.* Biochimica et Biophysica Acta (BBA)-Biomembranes, 2010. **1798**(3): p. 471-481.

48. Podobnik, M., et al., *Crystal structure of an invertebrate cytolysin pore reveals unique properties and mechanism of assembly.* Nature Communications, 2016. **7.** doi: 10.1038/ncomms11598

49. Yilmaz, N., et al., *Real-time visualization of assembling of a sphingomyelin-specific toxin on planar lipid membranes.* Biophysical Journal, 2013. **105(6)**: p. 1397-1405.

50. Yilmaz, N. and T. Kobayashi, *Visualization of lipid membrane reorganization induced by a pore-forming toxin using high-speed atomic force Mmicroscopy.* ACS Nano, 2015. **9**(8): p. 7960-7967.

51. Song, L., et al., *Structure of staphylococcal alpha-hemolysin, a heptameric transmembrane pore.* Science, 1996. **274**(5294): p. 1859-1866.

52. Fologea, D., et al., *Controlled gating of lysenin pores.* Biophysical Chemistry, 2010. **146**(1): p. 25-29.

53. Fologea, D., et al., *Bi-stability, hysteresis, and memory of voltage-gated lysenin channels.* Biochimica et Biophysica Acta, Biomembranes, 2011. **1808**(12): p. 2933-2939.

54. Fologea, D., et al., *Multivalent ions control the transport through lysenin channels.* Biophysical Chemistry, 2010. **152**(1-3): p. 40-45.

55. Fologea, D., et al., *Potential analytical applications of lysenin channels for detection of multivalent ions.* Analytical and Bioanalytical Chemistry, 2011. **401**: p. 1871-1879.

56. Zhang, L., R. Buchet, and G. Azzar, *Interactions of caged-ATP and photoreleased ATP with alkaline phosphatase.* Biochemical and Biophysical Research Communications, 2005. **328**(2): p. 591-594.

57. Fologea, D., et al., *Cationic polymers inhibit the conductance of lysenin Channels.* The Scientific World Journal, 2013. doi: 10.1155/2013/316758

58. Montal, M. and P. Mueller, *Formation of bimolecular membranes from lipid monolayers and a study of their electrical properties.* Proceedings of the National Academy of Sciences, 1972. **69**(12): p. 3561-3566.

59. Pedersen, P.J., et al., *Liposomal formulation of retinoids designed for enzyme triggered release.* Journal of Medicinal Chemistry, 2010. **53**(9): p. 3782-3792.

60. Larson, E.M., et al., *A new, simple, nonradioactive, nontoxic in vitro assay to monitor corneal endothelial cell viability.* Investigative Ophthalmology and Visual Sciences, 1997. **38**(10): p. 1929-1933.

61. Krewski, D., et al., *Human health risk assessment for aluminium, aluminium oxide, and aluminium hydroxide.* Journal of Toxicology and Environmental Health, 2007. **10**(sup1): p. 1-269.

62. Palmer, R.J., J.L. Butenhoff, and J.B. Stevens, *Cytotoxicity of the rare earth metals cerium, lanthanum, and neodymium in vitro: Comparisons with cadmium in a pulmonary macrophage primary culture system.* Environmental Research, 1987. **43**(1): p. 142-156.

63. Bryant, S., et al., *Purinergic control of lysenin's transport and voltage-gating properties.* Purinergic Signalling, 2016. **12**(3): p. 549-559

64. Schwiebert, E.M. and A. Zsembery, *Extracellular ATP as a signaling molecule for epithelial cells.* Biochimica et Biophysica Acta (BBA) - Biomembranes, 2003. **1615**(1-2): p. 7-32.

65. Frey, T., *Nucleic acid dyes for detection of apoptosis in live cells.* Cytometry, 1995. **21**(3): p. 265-274.

66. Belloc, F., et al., *A flow cytometric method using Hoechst 33342 and propidium iodide for simultaneous cell cycle analysis and apoptosis determination in unfixed cells.* Cytometry, 1994. **17**(1): p. 59-65.

67. Sanfilippo, S., et al., *Viability assessment of fresh and frozen/thawed isolated human follicles: reliability of two methods (Trypan blue and Calcein AM/ethidium homodimer-1).* Journal of Assisted Reproduction and Genetics, 2011. **28**(12): p. 1151-1156.

68. Sawa, A., et al., *Increased apoptosis of Huntington disease lymphoblasts associated with repeat length-dependent mitochondrial depolarization.* Nature Medicine, 1999. **5**(10): p. 1194-1198.

69. Papadopoulos, N.G., et al., *An improved fluorescence assay for the determination of lymphocyte-mediated cytotoxicity using flow cytometry.* Journal of Immunological Methods, 1994. **177**(1-2): p. 101-11.

70. Hiraoka, Y. and K. Kimbara, *Rapid assessment of the physiological status of the polychlorinated biphenyl degrader Comamonas testosteroni TK102 by flow cytometry.* Applied and Environmental Microbiology, 2002. **68**(4): p. 2031-2035.

71. Baumgart, J., et al., *Quantified femtosecond laser based opto-perforation of living GFSHR-17 and MTH53 a cells.* Optics Express, 2008. **16**(5): p. 3021-3031.

72. Mohanty, S.K., M. Sharma, and P.K. Gupta, *Laser-assisted microinjection into targeted animal cells.* Biotechnology Letters, 2003. **25**(11): p. 895-899.

73. Lei, M., et al., *Femtosecond laser-assisted microinjection into living neurons.* Journal of Neuroscience Methods, 2008. **174**(2): p. 215-218.

74. Bowman, A.M., et al., *Analysis of plasma membrane integrity by fluorescent detection of Tl(+) uptake.* The Journal of Membrane Biology, 2010. **236**(1): p. 15-26.

75. Brittain, H.G., *Submicrogram determination of lanthanides through quenching of calcein blue fluorescence.* Analytical Chemistry, 1987. **59**: p. 1122-1125.

76. Goldstein, S., C.M. Fordis, and B.H. Howard, *Enhanced transfection efficiency and improved cell survival after electroporation of G2/M-synchronized cells and treatment with sodium butyrate.* Nucleic Acids Research, 1989. **17**(10): p. 3959-3971.

77. Sharifi Tabar, M., et al., *Evaluating electroporation and lipofectamine approaches for transient and stable transgene expressions in human fibroblasts and embryonic stem cells.* Cell Journal (Yakhteh), 2015. **17**(3): p. 438-450.

78. Vetter, J., *Toxins of Amanita phalloides.* Toxicon, 1998. **36**(1): p. 13-24.

79. Lengsfeld, A.M., et al., *Interaction of phalloidin with actin.* Proceedings of the National Academy of Sciences, 1974. **71**(7): p. 2803-2807.

80. Le Bihan, T. and C. Gicquaud, *Stabilization of actin by phalloidin: a differential scanning calorimetric study.* Biochemical and Biophysical Research Communications, 1991. **181**(2): p. 542-547.

81. Dancker, P., et al., *Interaction of actin with phalloidin: polymerization and stabilization of F-actin.* Biochimica et Biophysica Acta (BBA)- Protein Structure, 1975. **400**(2): p. 407-414.

82. Cooper, J.A., *Effects of cytochalasin and phalloidin on actin.* The Journal of Cell Biology, 1987. **105**(4): p. 1473-1478.

83. Faulstich, H., et al., *Fluorescent phallotoxins as probes for filamentous actin.* Journal of Muscle Research and Cell Motility, 1988. **9**(5): p. 370-383.

84. Wulf, E., et al., *Fluorescent phallotoxin, a tool for the visualization of cellular actin.* Proceedings of the National Academy of Sciences, 1979. **76**(9): p. 4498-4502.

85. Okagaki, T., S. Higashi-Fujime, and K. Kohama, *Ca^{2+} activates actin-filament sliding on scallop myosin but inhibits that on Physarum myosin.* The Journal of Biochemistry, 1989. **106**(6): p. 955-957.

86. Kron, S.J. and J.A. Spudich, *Fluorescent actin filaments move on myosin fixed to a glass surface.* Proceedings of the National Academy of Sciences, 1986. **83**(17): p. 6272-6276.

87. Schmit, A.C. and A.M. Lambert, *Microinjected fluorescent phalloidin in vivo reveals the F-actin dynamics and assembly in higher plant mitotic cells.* Plant Cell, 1990. **2**(2): p. 129-138.

88. Corrotte, M., et al., *Toxin pores endocytosed during plasma membrane repair traffic into the lumen of MVBs for degradation.* Traffic, 2012. **13**(3): p. 483-494.

89. Keyel, P.A., et al., *Streptolysin O clearance through sequestration into blebs that bud passively from the plasma membrane.* Journal of Cell Science, 2011. **124**(14): p. 2414-2423.